

HIGH SPIN GLUEBALLS FROM THE LATTICE

H.B. Meyer¹, M.J. Teper²

Theoretical Physics, University of Oxford, 1 Keble Road,
Oxford, OX1 3NP, United Kingdom

We discuss the principles underlying higher spin glueball calculations on the lattice. For that purpose, we develop numerical techniques to rotate Wilson loops by arbitrary angles in lattice gauge theories close to the continuum. As a first application, we compute the glueball spectrum of the $SU(2)$ gauge theory in 2+1 dimensions for both parities and for spins ranging from 0 up to 4 inclusive. We measure glueball angular wave functions directly, decomposing them in Fourier modes and extrapolating the Fourier coefficients to the continuum. This allows a reliable labelling of the continuum states and gives insight into the way rotation symmetry is recovered. As one of our results, we demonstrate that the D=2+1 $SU(2)$ glueball conventionally labelled as $J^P = 0^-$ is in fact 4^- and that the lightest “J=1” state has, in fact, spin 3.

¹meyer@thphys.ox.ac.uk

²teper@thphys.ox.ac.uk

1 Introduction

There are several reasons to explore the higher spin spectrum of pure gauge theories. One might wish to test models of glueballs. Such models naturally divide into those where glueballs are composed of constituent gluons, for example the bag model (see [1] and references therein), and those in which glueballs are based on closed loops of chromo-electric flux, for example the Isgur-Paton flux-tube model [2]. Attempts to test these models [3 - 6] against existing lattice spectra are severely hampered both by the lack of lattice results for $J \geq 3$ in D=2+1 and $J \geq 4$ in D=3+1, and by ambiguities in assigning continuum spins to states that lie in representations of the lattice rotation group. Secondly, there has been a long-standing question in QCD phenomenology concerning the interpretation of the (soft) Pomeron within the low-energy spectrum. (See [7] for recent reviews.) The absence of a corresponding mesonic ($q\bar{q}$) trajectory has made glueballs the favoured candidates. Simple models [8] do indeed predict a Regge type behaviour of the glueball spectrum, namely $J \propto M^2$ at large J , with a slope that is much smaller than that of the usual mesonic Regge trajectories. A determination of the leading Regge trajectory in the pure gauge theory would largely resolve this issue. Thirdly, it is a generally interesting question to study how a symmetry that is broken on the lattice, in this case the rotation group, is restored as one reaches the continuum.

The standard method to measure the spectrum of a gauge theory is to evaluate the correlation function of a gauge-invariant operator in Euclidean space (for a review of “glueball technology”, see [9]):

$$\langle \mathcal{O}^\dagger(t) \mathcal{O}(t=0) \rangle = \sum_n |\langle 0 | \mathcal{O} | n \rangle|^2 e^{-E_n t} \quad (1)$$

This formula follows directly from the insertion of the complete set of energy eigenstates $|n\rangle$. In order to correctly label the latter with the quantum numbers of the rotation group, one has to construct operators that project out the undesired states. In continuum Euclidean space, it is possible to construct operators belonging to an irreducible representation of the rotation group; that is, with a definite spin. In two space dimensions, where, for simplicity, we shall work from now on, the construction amounts to

$$\mathcal{O}_J = \int \frac{d\phi}{2\pi} e^{iJ\phi} \mathcal{O}_\phi \quad (2)$$

where J is the spin and \mathcal{O}_ϕ represents an operator characterising the direction ϕ , i.e. \mathcal{O}_ϕ is obtained by rotating the operator $\mathcal{O}_{\phi=0}$ through an angle ϕ . If $|j; n_j\rangle$ is a state of spin j and other quantum numbers n_j , we have

$$\langle 0 | \mathcal{O}_J | j; n_j \rangle = \delta(J - j) \langle 0 | \mathcal{O}_\phi | j; n_j \rangle, \quad (3)$$

where ϕ is now arbitrary. The definite-spin subspaces in which the Hamiltonian can be diagonalised separately are still infinite-dimensional, so that extracting their lightest states requires an additional piece of strategy. The most commonly used is the variational method (see [9,10] and references therein), which tries to separate pure exponentials in eqn(1).

However, on a lattice, rotation symmetry is broken and only a handful of rotations leave the lattice invariant. Therefore physical states can only be classified into irreducible representations of the lattice point group. This is a much less thorough classification, in the sense that the diagonal blocks of the lattice Hamiltonian each contain a whole tower of smaller blocks of the continuum Hamiltonian. For instance, the trivial square lattice irreducible representation contains all multiple-of-4 spin states of the continuum, because $\exp\{iJ\phi\}$ is unchanged if $J \rightarrow J + 4n$, $n \in Z$, for any symmetry rotation of the lattice, i.e. for $\phi = n'\pi/2$, $n' \in Z$.

When extracting glueball masses from lattice calculations, it has been customary to label the obtained states with the lowest spin falling into the lattice irreducible representation; in the example above, it would be ‘spin 0’. Not only does the procedure used till now lack the capability of extracting the higher spin spectrum, but this labelling could very well be wrong, especially for excited states. Suffice it to think of the hydrogen atom, where the degeneracy in ℓ implies, for example, that the $n = 1, \ell = 1$ is lighter than the $n = 2, \ell = 0$ state. In the case of $D=2+1$ gauge theories, the simple flux tube model predicts [4,6] that the lightest $J^{PC} = 0^{-+}$ state is much heavier than the lightest 4^{-+} state, and the mass that it predicts for the latter agrees with the value obtained on the lattice [9] for the ‘ 0^{-+} ’. This suggests a possible misidentification, as emphasised in [4,6].

In the case of the 2 dimensional square lattice, the only states one can distinguish in the “traditional” fashion are those of spin 0, 1 and 2. This work is an attempt to go beyond that apparent limitation of lattice calculations: we want to check the correctness of the conventional labelling of states as well as to extract the lowest lying states carrying spin higher than 2. It is clear that one necessary ingredient in the realisation of this program is a reliable way to construct operators that are rotated with respect to each other by angles smaller than $\frac{\pi}{2}$ but that are otherwise (nearly) identical. Indeed one expects that as the lattice spacing becomes very much smaller than the dynamical length scale, this becomes possible due to the recovery of the continuum symmetries. In fact it has been known for a while that rotation symmetry is restored dynamically rather early in the approach to the continuum. An early piece of evidence came from the ($D = 3 + 1$) $SU(2)$ static potential measured off the lattice axis [12]. Later it was shown [13] that the ($D = 3 + 1$) $SU(3)$ glueball shown dispersion relation $E(\vec{p})$ to a good approximation depends only on $|\vec{p}|$ already at $\beta = 5.7$. The detailed glueball spectra obtained more recently in (2+1) [9] and (3+1) [14] dimensions exhibit the degeneracies between states belonging to different lattice irreducible representations that are expected in the continuum limit.

The outline of this paper is as follows. We begin by discussing techniques for constructing arbitrary rotations of a given operator. We design systematic tests to evaluate how well these methods perform in $D = 2 + 1$ $SU(2)$ gauge theory. (The generalisation to $SU(N)$ is trivial.) We then discuss how to use these techniques to extract the high spin spectrum from lattice simulations. As an example, we analyse the case of the lightest 4^- and 0^- glueballs. We find that the state conventionally labelled as a 0^- is in fact a 4^- , as was suggested by calculations of the spectrum within the flux tube model [4,6]. We also find that the $J = 3$ ground state is lighter than the $J = 1$ (again as suggested by the flux tube model). Although all our calculations in this paper are performed in two space dimensions, a large part of our motivation for studying this problem lies in $D = 3 + 1$ and we briefly discuss the application of our approach to that case. In the conclusions we briefly comment on some other recent attempts [15,16,17] to calculate the masses of higher spin glueballs and summarise our results. Our next step, to apply these ideas to determine the ‘Pomeron’ Regge trajectories in $SU(N)$ gauge theories, will be the subject of forthcoming publications.

2 Two methods of operator construction

Lattice glueball operators are usually constructed out of space-like Wilson loops. To construct lattice operators that project onto arbitrary spins we need linear combinations of Wilson loops

rotated by arbitrary angles. Since we are on a cubic lattice, such a rotated loop will usually only be an approximate (rotated) copy of the initial loop. The better the approximation, the less ambiguous the spin assignment. Now, a general Wilson loop consists of a number of sites connected by products of links. To obtain a good projection onto the lightest states in any given sector, these links need to be ‘smeared’ or ‘blocked’ so that they are smooth on physical rather than just ultraviolet length scales. (See, for example, [9] and references therein.) To construct arbitrary (approximate) rotations of various Wilson loops, it is clear that we need to be able to construct ‘smeared’ parallel transporters between arbitrary sites in a given time-slice of the lattice. We now describe two techniques to do this. We begin by reviewing and elaborating upon a method [11] that has recently been used [17] in an attempt to address the $0^-/4^-$ ambiguity referred to in the Introduction. This method is however too computationally expensive to allow a realistic continuum extrapolation with our resources, and without such an extrapolation one has very little control over the restoration of continuum rotational invariance. We therefore develop a second method that is much less expensive and provides a practical approach to the problem.

2.1 The matrix method

Consider the two spatial dimensions of a given time-slice of size $L \times L$ with periodic boundary conditions. Each point p is parametrised by integers (m, n) representing its Cartesian coordinates in lattice units. Given a mapping $i \rightarrow (m(i), n(i)) \equiv \varphi(i)$ and setting $N \equiv L^2$, we can define an $N \times N$ matrix M by its elements

$$M_{ij} \equiv U(\varphi(i); \varphi(j)) \quad (4)$$

where $U(p; q)$ is the link matrix joining points p to q if they are nearest neighbours, and vanishes otherwise. Since $U(p, q) = (U(q, p))^\dagger$, M is hermitian. For notational simplicity, if $\varphi(i)$ is the origin and $\varphi(j) = (m, n)$, we shall often write $M_{ij} \equiv M[m, n]$.

It is straightforward to see that $(M^\ell)_{ij}$ contains all paths of length ℓ going from $\varphi(i)$ to $\varphi(j)$. One can construct a “superlink” connecting these two points by adding up paths of all lengths, weighted by some damping factor that ensure the convergence of the series:

$$K = \sum_{\ell} c(\ell) M^\ell \quad (5)$$

In general it is very costly to calculate such a power series numerically. If one chooses $c(\ell) = \alpha^\ell$ then the series can be resummed

$$K = \sum_{\ell \geq 0} \alpha^\ell M^\ell = (1 - \alpha M)^{-1}. \quad (6)$$

and the calculation of the geometric series can be reduced to the inversion of a matrix. For instance, one can now compute a triangular “fuzzy” Wilson loop by simply multiplying together three elements of K

$$W = \text{Tr } K_{ij} K_{jk} K_{ki} \quad (7)$$

where i, j, k are the vertices of the triangle. It is clear that as we increase α the longer paths are less suppressed i.e. increasing α increases the smearing of the “superlink”. Thus by inverting a single matrix we obtain smeared parallel transporters between all pairs of sites in the given time-slice. We can now use these to construct any Wilson loops we wish.

While the above construction is valid for an infinite volume, one must be careful if the volume is finite. Consider, for example, the triangular Wilson loop defined in eqn(7). On a finite spatial torus, the sum of paths contributing to K_{ij} contains not only the ‘direct’ paths from i to j but also paths that go the ‘long’ way around the ‘back’ of the torus between these two points. That is to say, the Wilson loop defined in eqn(7) is not necessarily a contractible triangle; some of the contributions to W are non-contractible closed paths that wind once around the torus. In the confining phase such an operator projects onto flux loops that wind once around the torus. These states are orthogonal to glueballs. Moreover, in the kind of volume with which one typically works, this loop will be much lighter than any of the excited glueballs. Such effects induce an infra-red breaking of rotation symmetry that, unlike lattice spacing effects, will survive the continuum limit. Fortunately it is simple to modify our matrix procedure so as to explicitly suppress such contributions and we now describe two ways of doing so.

It is convenient to label the link matrix emanating from the site (x, y, t) in the direction μ by $U_\mu(x, y, t)$. Consider now the matrix M^x which is identical to M except that certain elements acquire a minus sign:

$$U_x(x = L, y, t) \rightarrow -1 \times U_x(x = L, y, t) \quad \forall y. \quad (8)$$

It is clear that the corresponding matrix K^x will produce ‘superlinks’ that are identical to those from K except that the contribution of paths that wind once (or an odd number of times) around the x -torus will come in with a relative minus sign. Thus if we replace K by $K + K^x$ in eqn(7) the contribution of all the non-contractible paths winding around the x -torus will cancel. In the same way we can define a matrix M^y from M by

$$U_y(x, y = L, t) \rightarrow -1 \times U_y(x, y = L, t) \quad \forall x \quad (9)$$

and a matrix M^{xy} which includes both the modifications in equations (8) and (9). It is easy to see that the sum of the corresponding inverse matrices, $K + K^x + K^y + K^{xy}$, will produce superlinks that have no contributions from non-contractible paths that wind around the x -torus or the y -torus or simultaneously around both tori. This is a simple and effective modification although it would appear to suffer from the fact that it quadruples the length of the calculation. However it is easy to see that one can considerably reduce this cost. We start by noting that on a lattice with an even number of sites in both x and y directions, even and odd powers of M connect a given point (say, the origin) to two disjoint sets of lattice sites. If L_x and L_y are odd, this is no longer the case, but paths joining two points by going around the world have an opposite parity weighting in powers of α to those connecting them directly. Therefore in that case we can proceed as follows: use $K_e \equiv (1 - \alpha^2 M^2)^{-1} = \sum_{n \geq 0} (\alpha M)^{2n}$ to propagate by an even number of lattice links and $K_o \equiv \alpha M K_e$ for an odd number of ‘jumps’. Thus paths with an odd winding number are excluded by construction. This way of proceeding has the additional advantage that one can truly propagate by a distance larger than $L_{x,y}/2$, which is not the case with $L_{x,y}$ even. On the other hand, the fact that with an even number of lattice sites in both directions K_e possesses a partitioned structure allows us to store any polynomial in the matrix M^2 in two matrices of size $L^2/2 \times L^2/2$. If standard inversion algorithms are applied to compute K_e (for which the CPU time scales as N^3), this represents a reduction in CPU time by a factor four. K_o is then very fast to obtain, given the sparsity of the matrix M . In summary, obtaining the superlinks free of odd winding number paths requires either of the following computations: if the lattice has an odd number of sites,

it is sufficient to perform one full matrix inversion, plus two multiplications by M ; if $L_{x,y}$ are even, we have to use the four $Z(2)$ transformations, as discussed above, but we can compute and store the superlinks in matrices smaller by a factor two.

There is an interesting interpretation to the matrix construction in an infinite volume. If we choose the mapping such that $\varphi^{-1}(m,n) = L \cdot m + n$, then in the frozen configuration (all link variables set to unity), M coincides with the matrix used in discretising partial differential equations in the finite difference scheme; more precisely, $M - 4$ is exactly the expression of a discretized Laplacian operator on a torus. For that reason, the Klein-Gordon equation $-\nabla^2 F + m^2 F = 0$ translates into

$$((am)^2 + 4 - M)_{ij} F_j = 0, \quad \forall i = 1, \dots, N \quad (10)$$

where F is now a column vector containing the approximate values of the function F on the lattice sites. If we introduce a point-like source $v^{(z)}$ on the RHS, that is $v_i^{(k)} = \delta_{ik}$, we obtain the interpretation that $[(am)^2 + 4 - M]^{-1}_{ij}$ is the $2d$ lattice propagator of a massive scalar field from point $\varphi(i)$ to point $\varphi(j)$. For a scalar field minimally coupled to the gauge field at finite β , the ordinary derivatives are simply replaced by covariant derivatives. If the scalar field is in the fundamental representation of the gauge group then our matrix $1 - \alpha M$ provides a discretisation of the kinetic term where the parameter α in eqn(6) corresponds to

$$\alpha = \frac{1}{(am_0)^2 + 4} \quad (11)$$

and m_0 is the tree level mass of the scalar particle. Setting α to $\frac{1}{4}$ corresponds to $m_0 = 0$. The propagator calculation amounts to introducing a scalar particle in the configuration, a ‘‘test-charge’’ that does not modify the configuration, but the closed paths of which reveal gauge-invariant information on the background gauge field. In other words, this method is analogous to performing a quenched simulation of the gauge theory minimally coupled to a scalar field (with the latter confined to a time-slice). The lighter the mass of the scalar particle, the greater the transverse distance that it explores as it propagates between two sites. That is to say, we recover our earlier conclusion: as α increases from small values, the propagator is increasingly ‘smearred’.

We expect on general grounds that if we calculate a propagator over some physical length scale, and for a mass am_0 that is fixed in physical units, then the lattice corrections to continuum rotational invariance will be $O(a^2)$. This provides a general theoretical argument that our matrix method will yield ‘rotationally invariant’ superlinks if one chooses the parameter α suitably. Of course, since there is no symmetry to protect against mass counter-terms, there will be both an additive and a multiplicative renormalisation of the mass. That is to say, choosing the mass involves a ‘fine-tuning’ problem that is very similar to the one that one encounters when using Wilson fermions.

The recovery of rotational invariance at large distances and at weak coupling can, in general, only be seen numerically (see below). However, in the special case of a frozen configuration, it can in fact be studied analytically (see Appendix A). This leads to the following conclusions: if $m^2 + n^2 = d^2$, for $1 \ll d \ll (am_0)^{-1}$ the propagation from $(0,0)$ to (m,n) results from a Brownian motion and the length of the dominating paths is of the order d^2 . In this regime rotation invariance is recovered. For $d \gg (am_0)^{-1}$ on the other hand, the superlinks become more directed and rotation invariance is lost. Since one should think of a frozen field configuration as corresponding to $\beta = \infty$, i.e. to the continuum limit $a = 0$, we

should take the mass to be $am_0 = 0$ if it is to be finite in physical units. In that case, only the range $1 \ll d \ll (am_0)^{-1} = \infty$ is relevant. If we wish to think of a very small but non-zero value of a , then the regime in which a frozen configuration is an approximation to the field is for $d \ll (am_0)^{-1}$, if m_0 is on the order of a physical length scale. In either case $d \gg (am_0)^{-1}$ does not correspond to a physically relevant range of distances.

The matrix method is a simple and powerful tool for obtaining smeared ‘superlinks’ between all pairs of sites in a given time-slice. However even in D=2+1 SU(2) and at moderate β values the matrix is already large and the inversion expensive. While a calculation with modest statistics on say a 16^3 lattice may be readily performed on a workstation, this is no longer the case for the 24^3 and 32^3 lattices that would be needed for even a minimal attempt at a continuum extrapolation. To circumvent this problem we develop a much faster alternative method in the next subsection. However, before turning to that, we finish with some general remarks about how the matrix method may be developed into a more realistic tool.

We have noted that the elements of our inverse matrix $K = (1 - \alpha M)^{-1}$ are nothing but the propagators of a minimally coupled scalar particle in the fundamental representation, whose bare mass is determined by the parameter α . In principle we are free to consider propagators of other particles: these should provide equally good ‘superlinks’. Consider then a fermion in the fundamental representation and suppose we discretise it as a two-dimensional staggered lattice fermion. The propagators are obtained by inverting a matrix which is obtained from our matrix M simply by multiplying the elements of M by position-dependent factors of -1 [18]. This lattice discretisation maintains a chiral symmetry which protects the massless fermions from an additive renormalisation. This removes the fine-tuning problem we referred to earlier: a first advantage. Moreover we expect the long distance physics to be encoded in the lowest eigenvalues, and corresponding eigenvectors, of our (discretised) Dirac operator. Now we recall that the fermion propagator can be expressed in terms of all the eigenvectors and eigenvalues of the Dirac operator. If we truncate this sum to include only some suitably chosen set of these lowest eigenvalues and eigenvectors, then this should provide us with an approximation to the propagators that maintains the long-distance physics; for example the restoration of full rotational invariance. That is to say, they can be used as ‘superlinks’ for our purposes. As we approach the continuum limit we do not need to increase the number of these eigenvectors, as long as the volume is fixed in physical units, so the computational cost scales in a way that is far better than inverting the full Dirac operator – a second, major, advantage. As an added bonus we note that we can expect the chiral symmetry to be spontaneously broken. This implies a non-zero density of modes near zero which generates the chiral condensate [19], and the choice of what are ‘small’ modes then becomes unambiguous. This is of course only an outline of a strategy; its practical application is something we do not attempt here.

2.2 The path constructor method

We turn now to a simpler, more direct and, above all, faster alternative method for constructing superlinks between any two sites.

In order to define a path from site A to site B , we first introduce a “d-link” in the diagonal direction of the lattice:

$$U_{\mu\nu}(x) = \mathcal{U} (U_\mu(x)U_\nu(x + a\hat{\mu}) + U_\nu(x)U_\mu(x + a\hat{\nu})) \quad (12)$$

where \mathcal{U} represents a unitarisation procedure (in $SU(2)$, the operation amounts to dividing

the matrix by its determinant). From a point x , there are now 8 directions available. It is easy to write an algorithm that finds the path following the straight line from A to B as closely as possible. Indeed, at each step, it is sufficient to try all directions by adding the corresponding (d-)link to the current state of the path and select the result that has maximal projection on the \overrightarrow{AB} vector. As this can lead to a path that is not invariant under a π -rotation, one can average with the opposite path obtained with the same algorithm by starting from B and inverting it at the end. In practise, before starting to calculate the path, we may, as usual, smear the ordinary links to reduce short-wavelength fluctuations and achieve better overlap onto physical states.

2.3 A test for the operator construction methods

We will now calculate appropriate Wilson loops using the two kinds of superlinks introduced above, so as to test the extent to which rotation symmetry is violated. The result is obviously determined by the dynamics of the lattice gauge theory and the operator being measured. Therefore, to obtain rotation invariance to a good accuracy, the two following conditions must be satisfied:

$$aL \gg \sigma^{-1/2} \quad \text{and} \quad \sigma^{-1/2} \gg a \quad (13)$$

It is our task, when constructing rotated copies of operators, to ensure that these conditions are also sufficient.

We will refer to the method using the propagator as “method I”, to the path constructor method as “method II”. In both cases, in order to have a gauge-invariant operator, we must form a closed path. Since a great number of paths contribute to the superlinks in method I, an operator of the type

$$\mathcal{O} = \text{Tr } K(y, x) \cdot K(x, y) \quad (14)$$

is a perfectly acceptable operator characterising the direction determined by the points x, y . We call it a “segment” operator. (It has an interesting physical interpretation which we shall elaborate upon below.) We can choose pairs of points x, y that have approximately the same length – up to the percent level – and which are rotated by an approximately constant angle. These “approximations” mean that there is an intrinsic limitation to the rotation invariance that we can expect to observe at a “fixed” length $|x - y|$. One can finesse this problem by plotting the values of $\mathcal{O}(x, y)$ for all points x, y and seeing to what extent they fall on a single smooth curve. For our purposes an alternative two-part strategy is more illuminating. In the first step, working at a “fixed” value of $|x - y|$, we ask if the violations in rotation symmetry are of the same order of magnitude as the differences in the lengths. In the second step, as a more direct test of rotational invariance, we first normalise the operators $\mathcal{O}(\phi)$ to a common value and then calculate the correlation between rescaled segment operators at different angles.

We perform these tests on a 16^3 lattice at $\beta = 6$, where we know [9] that the string tension is $a\sqrt{\sigma} \simeq 0.254$ so that the conditions in eqn(13) would appear to be satisfied. We choose $\alpha = 0.24$ and there is no preliminary smearing of the links. Using the tree-level relation in eqn(11) and the above value of $a\sqrt{\sigma}$ we see that this value of α corresponds to a mass for the scalar particle of $m_0 \simeq 1.6\sqrt{\sigma}$, i.e. a physical rather than an ultra-violet scale. The segment we use is of length $7a$, and is rotated by multiples of approximately $\frac{\pi}{16}$. To illustrate the necessity of the torelon-suppression procedure, we shall present our results with and without implementation of the latter.

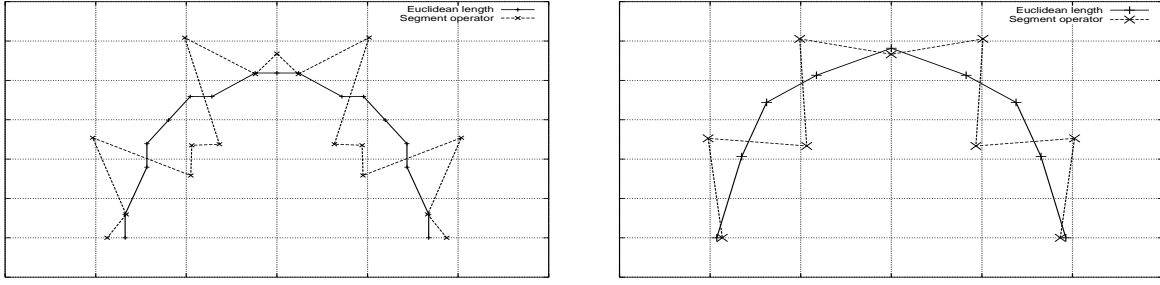


Figure 1: In polar coordinates: the Euclidean length and the average value of segment operators in different directions ϕ ; left: method I without torelon-suppression, right: method I with torelon-suppression

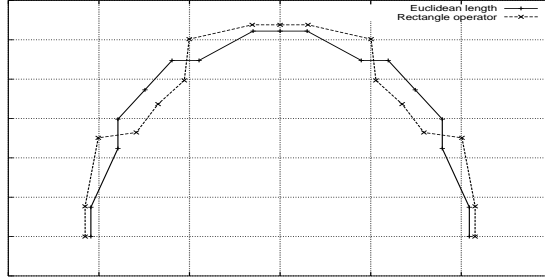


Figure 2: In polar coordinates: the Euclidean length and the average value of rectangle operators in different directions ϕ ; method II

We present in Fig. 1 the results of the first step of our test, as applied to method I. The points x, y that we use lie on an (approximate) semicircle and are joined by solid lines for clarity. We do not label the x and y axes, but the on-axis distance from the origin of the (semi)circle is 7 in lattice units and this sets the (separate) scales for the x and y axes. Using this information, the Euclidean length $R(\phi)$ of the segment in each direction ϕ can be read directly off this polar plot; the x-axis of the plot corresponds to the lattice x-axis. For each point x, y we plot the average value of the segment operator, as a point along the same direction, with the distance to the origin representing its value. For clarity these points have been joined up by dashed lines. Both sets of points have been rescaled so that they can be plotted on the same graph, and there are separate plots with and without torelon removal.

With method II, the superlink from a point A to a point B is a unitary matrix (or a sum of two such matrices). Therefore we cannot use segment operators since they would be trivial. Instead we use long rectangular Wilson loops, typically 7×1 ; they each characterise a specific direction ϕ . We present the results in Fig. 2 in a similar polar plot to that used in Fig. 1: in each direction ϕ , the Euclidean length $R(\phi)$ of the segment is given, as well as the average value of the rectangle operator pointing in that direction. Note that in this case there are no torelon contributions that need to be subtracted.

Remarks

Method I: The average operators have a significantly larger vacuum expectation value (vev) in the $\phi = \frac{\pi}{8}$ direction, and a smaller vev in the $\frac{\pi}{4}$ direction. Notice that the data is symmetric around the $\frac{\pi}{4}$ direction. The observed distortions are not due to winding paths, since the data with the torelon suppression implemented shows the same pattern.

Method II: Although there are still variations of the operators' vev's along the semicircle, they are of the same order as the geometric distortions. It must be said that the right angles of the rectangles also get distorted, so that in general, the rectangle becomes a parallelogram at an arbitrary angle ϕ .

The above comparison provides a first hint as to the rotational properties of these operators, although it is not as direct as it might be because the Wilson loops used for method I and method II are somewhat different. In the case of the segment operator used with method I, there is a simple and useful physical interpretation. As we saw earlier, the superlink $K(x, y)$ is the propagator of a scalar particle in the fundamental representation of the gauge group in two Euclidean dimensions. Its tree-level mass m_0 is given by eqn(11). Thus the segment operator in $\mathcal{O}(x, y)$ is the quenched propagator of 'mesons' composed of a scalar and its antiparticle. Such a point to point propagator includes contributions from all allowed energies and from excited as well as ground state masses. Since our value of α corresponds to $2am_0 \simeq 0.8$, the propagator will vary rapidly with distance. In addition, the short distance part of the propagator will certainly vary strongly with the angle ϕ . Note that if we were to use in the case of method I the same rectangular loops as we used for method II, then the physical interpretation would remain the same, except that the 'meson' wavefunctional would now be smeared, extending over roughly one lattice spacing, which one would expect to favour the contribution to the propagator of the lighter intermediate states, leading to a weaker dependence on distance.

In any case it is clear from the above that if we want to construct trial wave-functionals with definite rotational properties, then we should renormalise the individual operators $\mathcal{O}(\phi)$ in such a way that they have exactly the same vev. Doing so we shall now investigate how far we can restore rotational invariance by looking at the correlation between rescaled segment operators at different angles.

Correlation of rotated operators

Using the values of the segment operators calculated above, we calculate the correlation function

$$\langle \bar{\mathcal{O}}(\phi - \frac{\Delta\phi}{2}) \bar{\mathcal{O}}(\phi + \frac{\Delta\phi}{2}) \rangle \quad (15)$$

for a fixed $\Delta\phi$ (the bar indicates that the operators are now rescaled so that $\langle \bar{\mathcal{O}}(\phi) \rangle = 1$). This quantity is plotted in the direction ϕ in the polar plots in Fig. 3 and Fig. 4 for methods I and II respectively. Ideally it should be independent of ϕ .

Remarks Method I: without the torelon suppression, we see that for a small angle between the operators (first graph, $\Delta\phi = \frac{\pi}{8}$), the correlation function has only small variations, of the order of the errors and geometric length and angle variations. However for a larger angle (second graph, $\Delta\phi = \frac{\pi}{4}$), the variations are significantly larger. The worst case is the difference between the $\Delta\phi = \frac{\pi}{2}$ correlation of two segment operators along the lattice main directions or along the diagonals; here there is no geometric error on $\Delta\phi$ and hardly any ($\sim 1\%$) on the

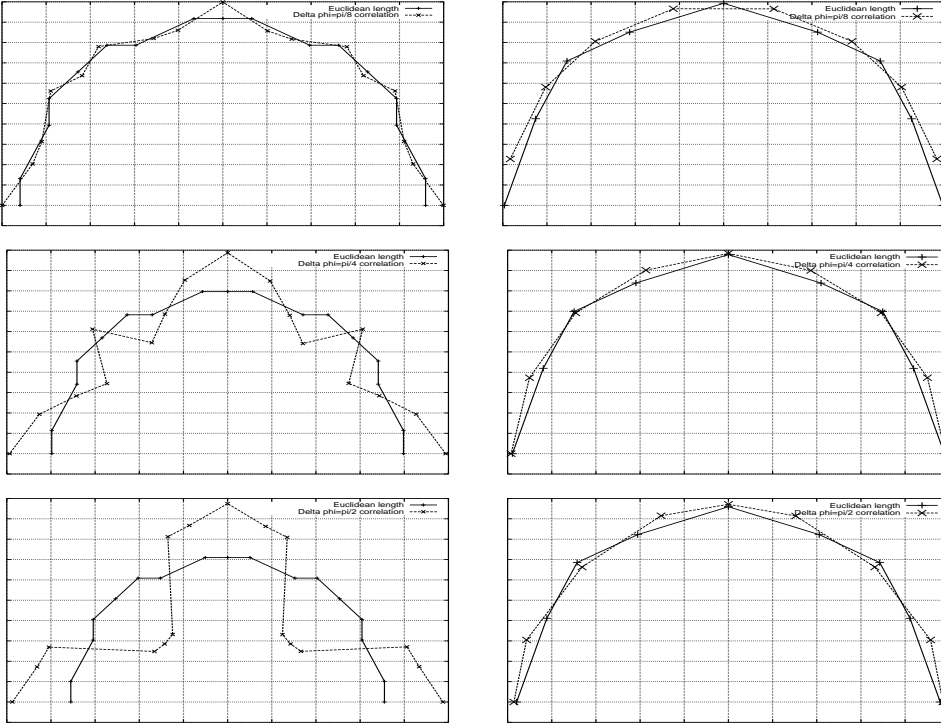


Figure 3: Method I: the Euclidean length and the correlation function (15) in different directions ϕ , for $\Delta\phi = \frac{\pi}{8}, \frac{\pi}{4}, \frac{\pi}{2}$ (from top to bottom); left: without torelon-suppression, right: with torelon-suppression.

length: yet the two correlation functions differ by a factor 2.5. This can be easily understood in terms of paths winding around the torus. Once the latter are suppressed (right column in Fig. 3), the rotation invariance is restored to a good approximation.

Method II: We notice that the correlation function is independent of ϕ , at the level of a few percent. In particular, the variations are practically the same at the three values $\Delta\phi = \frac{\pi}{8}, \frac{\pi}{4}, \frac{\pi}{2}$ and are of the same order as the geometric distortions.

Conclusion

The fact that we observe correlations between Wilson loops that are approximately independent of their orientation with respect to the lattice axes constitutes evidence for a dynamical restoration of rotation invariance. From the average values and correlation functions of rectangle operators constructed with a very simple algorithm, we conclude that both methods are suitable to calculate operators rotated by angles smaller than $\frac{\pi}{2}$. In view of the practical argument that method II is very much faster than method I, we shall use the former in practical calculations. Indeed, constructing the d-links takes less time than a smearing iteration, whereas the calculation of the propagator scales roughly as the sixth power of the lattice size.

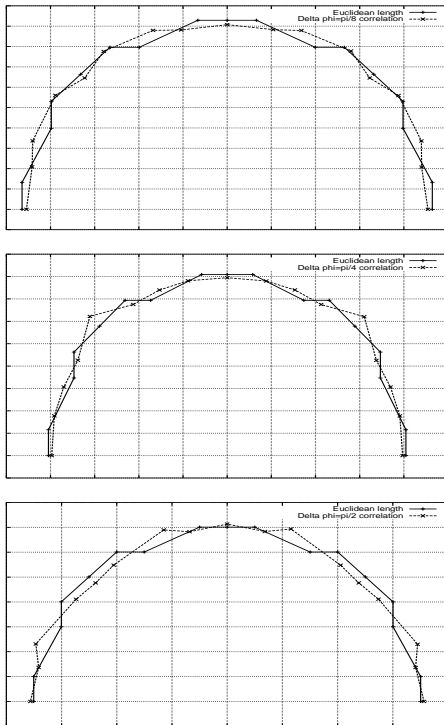


Figure 4: Method II: the Euclidean length and the correlation function (15) in different directions ϕ , for $\Delta\phi = \frac{\pi}{8}, \frac{\pi}{4}, \frac{\pi}{2}$ (from top to bottom)

3 High spin states on the lattice?

We now suppose that we dispose of a reliable way to construct operators rotated by angles of the type $\frac{2\pi}{n}$. How can we use this tool to resolve the spectrum of the theory in the continuum limit?

3.1 Lattice vs. continuum symmetry group

The symmetry group of the square lattice contains 2 rotations by $\frac{\pi}{2}$, one rotation by π and two types of symmetry axes (x and y axes, and $y = \pm x$ axes). For convenience, the character table of this group is given in appendix C. There are four one-dimensional representations, and one two-dimensional representation.

The continuum rotation group only has 1-dimensional irreducible representations (irrep's), due to the commutativity of rotations in the plane. However, because parity does not commute with rotations (see appendix B), we ought to consider 2-dimensional representations, which are irreducible under the full symmetry group (rotations + parity).

Each of the continuum two-dimensional representations can be decomposed onto the irreducible representations of the square. For instance, the spin 4^\pm representation D_4 decomposes onto two one-dimensional irreducible representations of the lattice group:

$$D_4 = A_1 \oplus A_2 \tag{16}$$

This tells us in what lattice irrep's to look in order to extract information on the D_4 states.

The Hamiltonian eigenstates belonging to A_1 can be written as linear combinations

$$|\psi_1\rangle = \sum_{n \geq 0} c_n(\rho) |(j = 4n)^+\rangle|_{lat} \quad \text{with} \quad \sum_n |c_n|^2 = 1 \quad (17)$$

and correspondingly for A_2

$$|\psi_2\rangle = \sum_{n \geq 0} c'_n(\rho) |(j = 4n)^-\rangle|_{lat} . \quad (18)$$

Here $|j^\pm\rangle$ are eigenvectors of both angular momentum and parity, the reference axis of which we have chosen to coincide with a lattice axis, and $|j^\pm\rangle|_{lat}$ denotes their restriction to the lattice sites. In other words, $\langle\phi|j^+\rangle \propto \cos j\phi$ and $\langle\phi|j^-\rangle \propto \sin j\phi$ (¹).

We now set ρ to a fixed physical length scale $\bar{\rho} \sim 1/\sqrt{\sigma}$. As we evolve from a small lattice spacing $a \ll \xi$ to coarser and coarser lattices, we imagine the following scenario in terms of the coefficients $c_n \equiv c_n(\bar{\rho})$:

- close to the continuum, for any particular Hamiltonian eigenstate $\psi_1 \in A_1$, the c_n are close to δ_{mn} for some m . If for instance $m = 1$, these states “remember” that their wave function changes sign under approximate $\frac{\pi}{4}$ rotations that are available on the lattice at length scales much greater than a . Moreover, the state in A_2 with $c'_n \simeq \delta_{nm}$ is almost degenerate with ψ_1 .
- as we move away from the continuum, the sharp dominance of one particular c_n in the series becomes smoother, and we can think of the angular wave functions as having a “fundamental mode” m , plus some fluctuations due to “higher modes”. It is as if we started with a sound of pure frequency, and the effect of the lattice is to add contributions from higher harmonics, giving the sound a richer timbre. The degeneracies between the states in A_1 and A_2 are broken more and more badly. This is due to the nonequivalence of the two classes of parity transformations available on the lattice.
- in general, more and more terms contribute to the series in eqn(17). Thus it seems that the angular dependence of a general state in A_1 or A_2 becomes very intricate. However as $a \rightarrow \xi$, higher modes in the expansion must become irrelevant, because there are no lattice points to support their fluctuations on the length scale of the theory. We know from the strong coupling expansion that the lowest lying states have a simple behaviour as $\beta \rightarrow 0$: the wave function of the fundamental state is simply a plaquette.

In fact, we have ignored a possible complication. We have assumed that no phase or roughening transition occurs, and that we can define smooth trajectories of the states in an E vs. a plane. However, in general we must expect crossings of states to occur. For any given range of energies, $E \leq E_0$, there will exist a lattice spacing a_0 such that for $a < a_0$, there are no more crossings until the continuum is reached². At a_0 , the states represent the continuum spectrum faithfully, with only small numerical deviations on their energies. We now follow the trajectory of one particular state as the lattice spacing is increased. Suppose we meet another

¹The $|0^-\rangle$ state is somewhat special in that it cannot be represented as the wavefunction of an object containing a symmetry axis. We shall exploit this property later on.

²There is a possible exception to that: we know that states come as parity doublets, which means that pairs of trajectories must converge and could possibly cross many times in doing so. This is not a problem for the present discussion.

trajectory at $a = a_1$. At that particular lattice spacing, there will seem to be an “accidental” degeneracy. Nearly-degenerate states will mix with the mixing driven by the matrix element of the lattice Hamiltonian between the ‘unperturbed’ eigenstates, i.e. $\langle 1|H(a)|2\rangle$. Near the continuum limit the unperturbed states will be close to continuum spin eigenstates, $H(a)$ will be close to the continuum Hamiltonian and so the mixing parameter $\langle 1|H(a)|2\rangle$ will be close to zero. Nonetheless sufficiently close to the crossing, the states will mix completely and so will the angular Fourier components of the state. That is to say, the Fourier components need not have a simple behaviour with a as $a \rightarrow 0$, and care must be taken to identify any near-degeneracies in following the Fourier components toward the continuum.

3.2 Two strategies

With these ideas on the evolution of the rotation properties of the physical states as functions of a , at least two (related) strategies are available in order to extract the high spin continuum spectrum numerically:

- I. if we can afford to work close to the continuum, we can construct operators with an approximate continuum wave function (cwf) $e^{iJ\phi}$, using the operator construction technique presented earlier. This kind of operator belongs to one of the irreducible representations of the lattice symmetry group. But because the perturbation of such an operator off the cwf is different from that of the Hamiltonian eigenstates, the expected behaviour of the local effective mass in the correlation function is the following: we should see an almost-flat plateau (corresponding to the excited state of the lattice irrep that will evolve into a high spin state in the continuum limit), followed by a breakdown into another, flat and stable plateau (corresponding to the fundamental state in the given lattice irrep).
- II. First we construct a set of lattice irrep operators, $\{W_i^1\}_{i=1}^N$. Next we construct (approximate) rotated copies of these. We thus have a large basis of operators, W_i^r , r labelling the rotation. We diagonalise the correlation matrix (using the variational method [10]) of $\{W_i^1\}_{i=1}^N$ in order to extract the energy eigenstates in this lattice irrep. These states ψ_i^1 are encoded by their components in the original basis W_i^1 :

$$\psi_i^1 = \sum_j v_{ij} W_j^1 \quad (19)$$

Now we need to determine the angular wave function of these glueball states. We do so by building the linear combinations

$$\psi_i^r = \sum_j v_{ij} W_j^r, \quad \forall r \quad (20)$$

and looking at the correlation function

$$G_t(r, r') = \langle \psi^{r_i \dagger}(0) \psi_i^{r'}(t) \rangle . \quad (21)$$

In practise the time-separation t is chosen so that the local effective mass of the ψ_i^1 2-pt function has reached a plateau. If we are reasonably close to the continuum, we should observe an approximate cwf behaviour of this correlation function, i.e. $G_t(r, r') \propto e^{iJ(\phi_r - \phi_{r'})}$ for some J , with small fluctuations of other modes (cf. eqn(17)). (As remarked above, care has to be taken near any level crossings.) Note that in principle this method can be generalised so that the operators used in eqn(21) are based on different loops.

We note that the data needed for both analyses is the same, so that they can easily be used in parallel. The second method has the advantage that there is no need to restrict ourselves to $\frac{2\pi}{n}$ -type angles in order to project out states corresponding to unwanted spins. On the other hand, if high spin states are very heavy, a large number N of trial operators will be needed in order that the variational method can resolve them. A simple case of this method, that does not employ the variational method and allows one to determine the mass and quantum numbers of the lowest-lying state in a given lattice irrep, consists in measuring the correlation matrix of one operator W with its rotated copies $\{W^r\}$ at sufficiently large Euclidean-time separation so that the local effective mass has reached a plateau.

3.3 A caveat

Before we present our actual results, we first illustrate how one can easily be misled by a naive application of ‘strategy I’. In the continuum, the simplest operator coupling to 4^+ , but not to 0^+ states, is the linear combination of two square Wilson loops rotated by 45 degrees with a relative minus sign. At $\beta = 6$ on a 16^3 lattice for instance, we might choose a set of four square-shaped operators:

	Squares:
1	$(4, 0) \pm (3, 3)$
2	$(5, 0) \pm (4, 4)$
3	$(6, 0) \pm (4, 4)$
4	$(7, 0) \pm (5, 5)$

The notation here is that each pair of points represent the coordinates of the end of a side of the square that begins at the origin. This specifies the operator uniquely since we sum all translations of the square in forming zero momentum operators. The \pm sign determines whether the linear combination of the two squares is a trial $J = 0$ or $J = 4$ operator. We calculate these operators using the M matrix method with $\alpha = 0.24$. If we diagonalise the four 4^+ operators according to the variational procedure [10], we obtain the following components of the two lightest operators (primed) in the normalised initial basis (unprimed):

components	1	2	3	4	am (1 lat. sp.)
$1'$	-0.97	7.2	3.7	-0.89	1.754(58)
$2'$	-1.6	18.2	-13.8	0.32	1.882(46)

Must we conclude that $am = 1.754$ is an upper bound on the lightest 4^+ glueball mass at $\beta = 6$? In fact, these masses are completely compatible with the masses of the 0^{+*} and 0^{+**} obtained in [9]. Indeed, the equal-time overlaps of the operators $1'$ and $2'$ onto our best ‘ 0^+ ’, ‘ 0^{+*} ’ and ‘ 0^{+**} ’ operators, obtained from the variational method, are found to be $(-0.13, 0.98, -0.04)$ and $(0.096, 0.16, -0.12)$ where the operators have been normalised in such a way that their equal-time 2-pt function is 1. This clearly shows that the correlator of the candidate ground state ‘ 4^+ ’ operator yields nothing but the 0^{+*} mass. A possible explanation of how it can be so is the following. The very smeared squares constructed here with superlinks “look” almost like rings of different sizes. Thus the relative minus signs in the linear combinations of the orthogonalised operators would suggest a radial wave function for the glueball that contains nodes and what we have actually constructed are operators suited to measure excited 0^+ states.

Thus the naive application of the continuum notion of 'spin' can lead to a wrong labelling of the states extracted from the lattice. The general point is that since the rotated loops are only approximate copies of each other, it is quite possible that the cancellations induced by the oscillating coefficients induce not only a piece of the wavefunction that has the desired angular oscillations, but also a piece where the cancellations, and resulting oscillations, are in the radial rather than angular direction. The latter can project onto an excited 0^+ . (Since one expects the ground state radial wavefunction to be smooth, a significant overlap onto the ground state 0^+ would be unexpected.) Now, since the lightest 0^+ is very much lighter than the lightest 4^+ , even such an excited 0^+ may be lighter than the lightest 4^+ – as turns out to be the case here – and may undermine a variational calculation. As $a \rightarrow 0$ and the rotated loops can be chosen to be better copies of each other, the radial cancellations become more extreme, the 0^+ states being projected upon become more highly excited and more massive, and once they become more massive than the lightest 4^+ states of interest the problem disappears for all practical purposes. The general lesson is that one can never be completely confident that one has isolated a high spin state at a fixed value of a . It is only through varying a toward the continuum limit that such confidence can be achieved.

4 Applications of Strategy I

As remarked in the Introduction, a robust prediction [4,6] of the Isgur-Paton flux tube model [2] is that the lightest 0^- state should be much heavier than the mass that has been obtained in lattice calculations [9] of the lightest SU(2) glueball in the A_2 lattice representation. Moreover the latter mass is close to the mass of the 4^- glueball as predicted by the flux tube model [4,6]. Since the A_2 lattice representation contains the continuum 0^- , 4^- , ... states this has led to the conjecture [4,6] that the lightest A_2 state is in fact 4^- rather than 0^- . All this has motivated some lattice calculations [15,17] which suggest that this is in fact so.

In this Section we shall use the first of the two strategies outlined in Section 3.2 to address this question in some detail. We shall begin with a simple approach applied directly to states in the A_2 representation (the conclusions of which will be confirmed in a quantitatively controllable way when we apply 'strategy II'). The reader will note that the approach we use here is similar to the one we presented earlier as a caveat of how a naive approach can fail. However in that earlier example it was applied to the A_1 representation where the 4^+ state that we were trying to isolate is much heavier than the lightest, and first excited 0^+ states. Here by contrast the candidate 4^- state turns out to be much lighter than the 0^- , so that it is the A_2 ground state that is being identified as 4^- . Now, as pointed out in Section 3.3, we do not expect a significant projection of a trial 4^- operator onto the 0^- ground state. Since we expect the A_2 ground state to be either the 0^- or the 4^- ground state, it must in fact be the latter. Thus in this rather special case, which will not be characteristic of other high spin calculations, our caveat loses its force.

We then return to the more difficult question of how one isolates the 4^+ from the 0^+ in the A_1 representation. We provide a procedure that appears to work well. Because of parity doubling for $J \neq 0$ this provides another way to calculate the 4^- mass. (And indeed the 4^+ and 4^- masses we obtain are entirely compatible.) After checking that finite volume corrections for the higher spin states are under control, we perform calculations for several larger β values and extrapolate our mass ratios to the continuum limit, as one needs to do if one is to be confident that one has indeed separated the different spin states.

Simulation details.- All our calculations use the standard Wilson action. The update is a 1:4 mixture of heat-bath ([22], [23]) and over-relaxation [24] sweeps. Because we measure a large number of operators, we can do 6-8 of these compound sweeps between measurements without significantly increasing the total cost of the calculation. We use an increasing number of smearing [21] iterations (and also increase the smearing weights) as we approach the continuum. For the lattice data that we eventually extrapolate to the continuum (Tables 2 and 3), we perform $\mathcal{O}(10^5)$ sweeps and collect the data typically in 30 bins. Errors are estimated with a standard jackknife analysis.

4.1 The $0^- / 4^-$ puzzle

To distinguish the 0^- from the 4^- glueball we construct trial 0^- and 4^- wavefunctionals using suitable linear combinations of (approximate) rotated copies of asymmetric operators (as described earlier). We first do this for a set of three operators and their twelve rotations. We simultaneously calculate operators in the A_2 lattice representation that are of the same kind as were used in [9], where it was assumed that the lightest state was the 0^- . We find that the overlap of these A_2 operators is large onto our trial 4^- operators and small onto the 0^- ones. In addition the mass of the former is much lighter than the mass of the latter. This strongly suggests that the lightest A_2 state becomes the 4^- glueball in the continuum limit.

Subsequently, we use two further independent sets of operators, each rotated eight times, so as to obtain an extra check on our calculation. The masses obtained at one lattice spacing are found to agree within errors.

The calculations in this subsection are performed at $\beta = 6$ on a 16^3 lattice. The links are smeared before the paths joining lattice sites are constructed.

Twelve-fold rotated operators.- The three operators on the left of Fig. (5) are rotated through 12 angles while maintaining, approximately, their shapes. Those on the right – which are only rotated by 90 degrees – are of a type that has been used previously [9] to measure the lightest state in the A_2 representation. With the former three operators and their rotations, we form linear combinations that correspond to trial 4^- and 0^- operators, while with the latter three operators we construct the A_2 representation of the square group. We now look at the overlaps between these two sets of operators. The overlap here is defined as

$$\text{overlap} \equiv \frac{\langle \mathcal{O}_1 \mathcal{O}_2 \rangle}{(\langle \mathcal{O}_2 \mathcal{O}_2 \rangle \langle \mathcal{O}_1 \mathcal{O}_1 \rangle)^{\frac{1}{2}}} \quad (22)$$

and the values we obtain are:

overlap	1(A_2)	2(A_2)	3(A_2)
I(4^-)	0.89	0.88	0.73
II(4^-)	0.95	0.96	0.97
III(4^-)	0.38	0.38	0.24
I(0^-)	0.24	0.20	0.15
II(0^-)	-	-	-
III(0^-)	0.16	0.13	< 0.01

The horizontal labelling refers to the three A_2 operators based on the three loops on the right of Fig.5, while the vertical labels are the three ‘ 4^- ’ and ‘ 0^- ’ operators obtained using the left-hand loops. (Errors are smaller than 1% here; shape II produced a very noisy 0^-

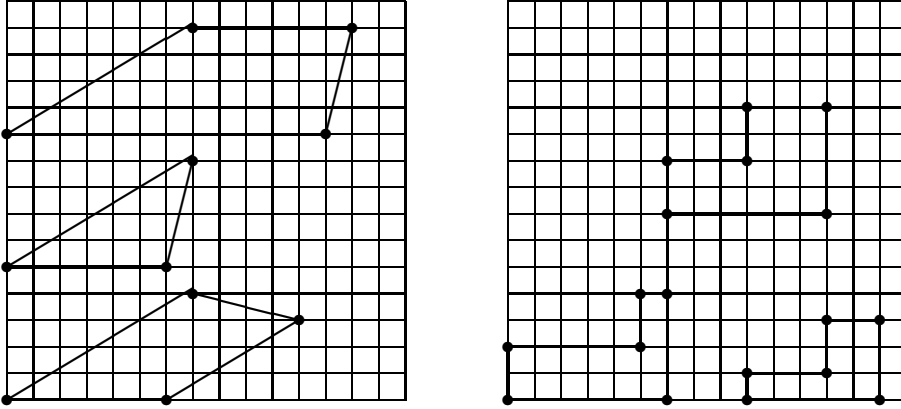


Figure 5: On the left, operators used to construct a 4^- wave function; (I) trapeze (II) triangle (III) pentagon. On the right, a “conventional” set of operators (1) bottom left (2) top (3) bottom right

operator.) Clearly, the approximate 4^- operators overlap much more onto the operators of the A_2 representation. This, and the fact that we observe a much smaller mass for our trial 4^- operator than for the 0^- , is a strong indication that the labelling in [9] of the lightest A_2 glueball as 0^- was mistaken, and that it is in fact a 4^- . Performing a variational analysis of the correlation matrix of the first set of operators, we obtain effective masses at one lattice spacing of $am(4^-) = 2.556(68)$ and $am(0^-) = 3.34(31)$. The much larger error on the latter is a reflexion of a much poorer signal. At this stage it would be useful, as a check, to use the usual variational calculation to identify the lightest few 4^- and 0^- states, so as to verify explicitly their small mutual overlaps. However the very heavy 0^- mass discourages us from attempting a variational identification of excited 0^- states.

Eightfold rotated operators.- As a check we now repeat the above analysis using the quite different set of operators drawn in Fig. (6). There are two parallelograms, and three completely asymmetric shapes. We rotate them by 45 degree angles, so each is rotated 8 times, along with the parity images. Proceeding as before to construct approximate 4^- and 0^- wave functions, we extract masses at one lattice spacing of $am(4^-) = 2.519(52)$ and $am(0^-) = 3.016(42)$. We see that these estimates agree within errors with our earlier estimates. Thus we have obtained a consistency check, namely that the mass estimates and labelling are independent of the particular set of operators we are using.

Square operators.- Yet another evaluation of the lightest A_2 state is provided by the operators shown in Fig. (7). There are two squares and one rectangle. This time the mass at one lattice spacing is $am(4^-) = 2.610(65)$; again consistent with our earlier values.

4.2 The even-spin spectrum at $\beta = 6$

We now return to the problem of distinguishing 4^+ and 0^+ states in the A_1 representation. Since the 0^+ is much lighter than the 4^+ there is the danger that what we will claim to be

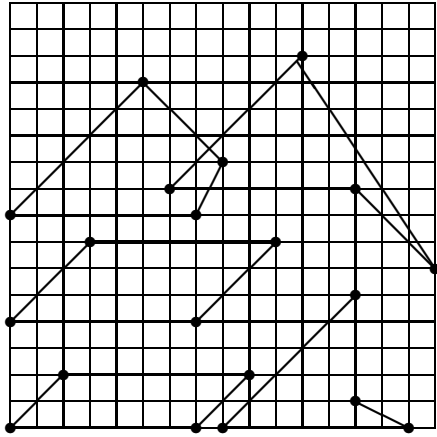


Figure 6: The operators used to construct 4^- and 0^- wave functions

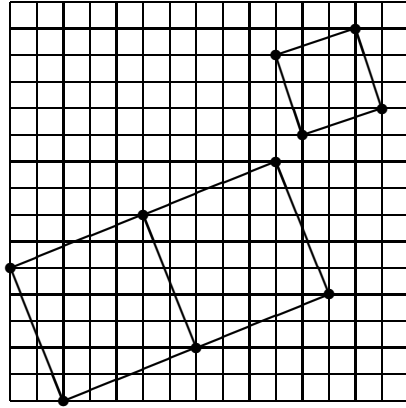


Figure 7: The square operators used for the A_2 representation

a 4^+ will in fact be an excited 0^+ ; as we warned in Section 3.3. Thus one needs to perform enough checks to avoid such a fate. This leads to a rather involved procedure which we will describe in the context of a calculation at $\beta = 6$. After checking that finite volume corrections on our higher spin masses are insignificant, we perform higher β calculations so as to be able to perform a continuum extrapolation.

To construct our trial states of spin 0 and 4 we use the four operators in Fig. (8) together with their twelve rotations. (Their coordinates can be found in Table 1).

4.2.1 A recipe for data analysis

We construct approximate rotations of the four shapes given above and we suppose that we have obtained the correlation of each operator in any orientation with any operator in any orientation. How can we separate with confidence the 4^+ from the 0^+ signal? Our experience has shown the following procedure to be reliable at $\beta = 6$. While the appropriate choice

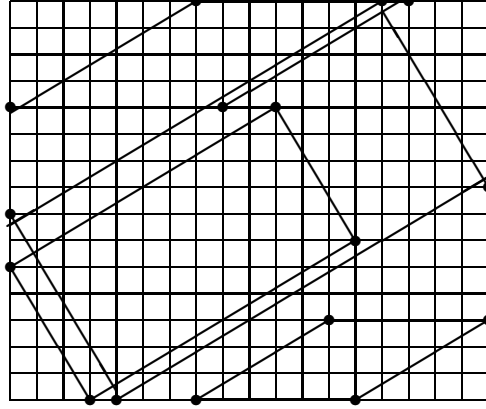


Figure 8: The operators used for the determination of the even spin spectrum; (1) small rectangle (2) large rectangle (3) small parallelogram (4) large parallelogram

of various selection parameters is empirical, in the continuum limit the procedure should be unambiguously valid if these parameters are made to approach obvious limiting values, and if the operators used are scaled appropriately and are chosen to be increasingly better copies of each other.

Preselection of the operators.- Look at the correlation matrix of each individual 'shape' with its rotated copies. This $n \times n$ matrix should (ideally) be a symmetric Toeplitz one, with the additional cyclic property ($M_{i,j} = M_{n+2-i,j}$, $i = j + 1, \dots, n$, reflecting the fact that the correlation between angle 0 and $\frac{2\pi}{n}$ is the same as between $-\frac{2\pi}{n}$ and 0. For instance, in the present case the correlation matrices of the operators read (op. 1 is top left, 2 top right, 3 bottom left and 4 bottom right):

1.00						1.00					
0.52	1.00					0.22	1.00				
0.24	0.52	1.00				0.26	0.22	1.00			
0.18	0.22	0.62	1.00			0.03	0.01	0.16	1.00		
0.22	0.13	0.22	0.52	1.00		0.01	0.00	0.01	0.21	1.00	
0.62	0.22	0.18	0.24	0.52	1.00	0.16	0.01	0.03	0.26	0.22	1.00
1.00						1.00					
0.84	1.00					0.65	1.00				
0.73	0.86	1.00				0.47	0.69	1.00			
0.60	0.65	0.87	1.00			0.37	0.42	0.69	1.00		
0.65	0.60	0.73	0.84	1.00		0.42	0.37	0.48	0.65	1.00	
0.87	0.73	0.76	0.73	0.86	1.00	0.69	0.48	0.49	0.48	0.69	1.00

Notice that the second is worse than the others; we therefore discard it and only operators 1, 3 and 4 remain in the subsequent steps.

Selection of the operators.- We now concentrate on the linear combinations corresponding to spin J_1 and spin J_2 operators (with $J_1 = 0$ and $J_2 = 4$ being the case of interest

here). Each of the spin J_1 operators has a certain overlap with each of the spin J_2 operators. This is due partly to the imperfect rotations, and partly because the lattice Hamiltonian eigenstates do not diagonalise the spin operator. First look at the diagonal quantities, that is the overlap of the J_1 and J_2 operators constructed with the same shape. Eliminate those which have more than $\sim 20\%$ overlap. (As $a \rightarrow 0$ the cut-off should gradually be reduced to zero as well.) Once bad operators are eliminated, this whole set of overlaps should contain none larger than 20% . If this cannot be achieved, it either means that we are too far from the continuum – in the sense that the wave functions of the physical states are very different from the continuum ones –, or that our rotated operators are not sufficiently faithful copies of the initial ones. In the present case, we find the following overlaps for our three candidate J_2 operators onto the corresponding J_1 operators: (0.04,0.0,0.12), (0.13,0.20,0.07) and (0.09,0.05,0.10) respectively for 1, 3 and 4, and so we retain these operators for the subsequent calculation.

Diagonalisation of the J_1 operators.- We now diagonalise the remaining n_{sel} J_1 operators using the variational procedure. To decide how many of the orthogonal states one should keep, the following criteria can be applied. From the comparison of the components of each linear combinations to $\chi \equiv (\det O)^{1/n_{sel}}$, where O is the transformation matrix leading to the orthogonal operators with unity equal-time correlator, only keep those lightest states whose components are not significantly larger than this determinant³. In practise, linear combinations with large components are found to have a very poor signal. In the present case, the coordinates in units of χ read (0.090, 0.24, 0.37), (0.37, -1.1, 1.1) and (-0.93, -1.19, 1.7); we keep all three states.

An intermediate check.- Look at the overlaps $\langle \mathcal{O}_{J_2} \mathcal{O}_{J_1}^D \rangle$. Here the $\mathcal{O}_{J_1}^D$ are the operators obtained from the variational procedure, and correspond to our best estimates of the relevant (i.e. the lightest) J_1 glueball wavefunctionals. The operators \mathcal{O}_{J_2} are the original un-diagonalised (but normalised) $J = 1$ loop combinations. We require that the total overlaps, which can now be calculated as

$$\left(\sum_i \left(\langle \mathcal{O}_{J_2} \mathcal{O}_{J_1}^{(D)i} \rangle \right)^2 \right)^{1/2}, \quad (23)$$

are less than 10 – 15%. Again we should take this cut-off $\rightarrow 0$ as $a \rightarrow 0$. The overlaps in the present case are (0.07,0.21,0.26), (0.14,-0.21,-0.38) and (0.088, 0.10, 0.039). Therefore we only keep the last operator as a candidate J_2 operator.

Diagonalisation of the J_2 operators.- Diagonalise the J_2 operators. In the present case the operation is trivial since we are left with only one operator.

Final check.- Now consider the same overlaps as above but with both J_1 and J_2 operators being diagonalised ones. The total overlaps between these final J_1 and J_2 operators is required to be still less than $\sim 20\%$ ($\rightarrow 0$ as $a \rightarrow 0$). Here we obtain a total overlap of 14%.

³If the determinant itself is large, try removing shapes that could be too similar to one another and diagonalise again.

4.2.2 Results

We give our results in terms of effective masses at 1 and 2 lattice spacings (see Table 2). The “quality” of an operator is defined as $|\langle \Omega | \mathcal{O} | n \rangle|^2$, where n is the state being measured and \mathcal{O} is our operator. In calculating this quantity we assume that the bold-faced mass values in the Tables represent the corresponding mass plateaux. The “overlap” calculates the overlap, as defined in equation (22), between the state of interest and each of the other spin eigenstates lying in the same square irreducible representation (e.g. spin 4 with the various spin 0 states obtained through the variational procedure) and adds these in quadrature. Thus it provides a measure of the overlap of the wavefunctional onto the basis of states of the ‘wrong’ spin.

We note that our operator construction method leads to excellent overlaps onto the physical states, while the overlaps of operators with different quantum numbers typically remain well under the 10% level. This quality requirement is obviously dependent on the spectrum itself: if there is a large gap between the spin 0 and the spin 4, the spin 4 operator will have to be of exceptionally high purity, since the heavier state contribution to the correlator, even with a much larger projection onto the operator, becomes negligible with respect to the lighter state at large time-separations.

4.3 Finite volume corrections

In physical units the size of our standard spatial volume is $aL \simeq 4/\sqrt{\sigma}$. This is the same size that was used in [9], where the choice was motivated by an explicit finite volume study, showing this to be more-or-less the smallest volume on which the lightest states in the A_1 and A_3 lattice irreducible representations did not suffer significant finite volume corrections. Since we would expect that the size of a glueball grows with its spin J , at least for large enough J , it is important to check that our volumes are indeed large enough to accommodate a glueball with $J = 4$.

We have therefore carried out an explicit check of finite volume effects at $\beta = 9$. Here $1/\sqrt{\sigma} \simeq 6a$, so our standard lattice size corresponds to $L = 24$. To check for finite volume corrections we also perform calculations on $L = 16$ and $L = 32$ lattices. The results are shown in Fig.9 and listed in Table 4. We see that there is no sign of any substantial correction to the $J = 4$ glueball mass between $L = 16$, $L = 24$ and $L = 32$, confirming that our mass calculations in this paper are not afflicted by significant finite volume corrections.

While this reassures us that our ‘standard’ volume size can be used safely at other values of β , it might seem paradoxical that we see no volume corrections on the smaller $L = 16$ lattice where the corrections to the $J = 2$ glueball mass are quite visible (in Fig. 9). This is in fact less odd than it appears. The reason is that the leading finite volume corrections to the $J = 2$ mass arise from the presence of states composed of pairs of flux tubes that wind around the spatial torus [9]. The mass of such a winding state is approximately $\propto L$ and as we decrease L it will at some point mix with the ‘true’ glueball state and then become lighter than it. (The same occurs at smaller values of L in the $J = 0$ sector). Thus the appearance of finite volume effects in the $J = 2$ sector should not be taken as a signal that the volume has become too small to accommodate that glueball and has no immediate implications for finite volume corrections for states of other spins.

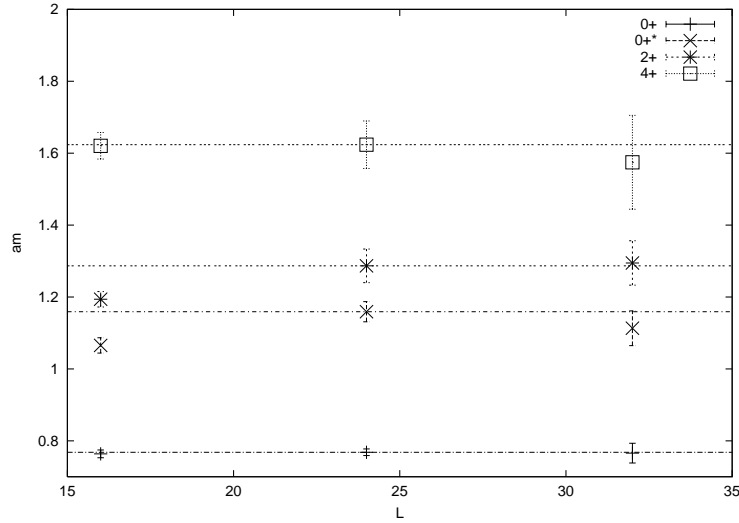


Figure 9: Volume dependence of some of the glueball masses at $\beta = 9$; the horizontal lines going through the data points at $L = 24$ are drawn to guide the eye.

4.4 Smaller lattice spacings and the continuum limit

Following the same procedure as we used for our $\beta = 6$ calculation in section 4.2.1, we perform further mass calculations at $\beta = 9, 12$ and 14.5 on lattices of the same physical size. The operators used are described in Table 1 and the results of our calculations are presented in Table 2. We now express the glueball masses in units of the string tension, $am/a\sqrt{\sigma} \equiv m/\sqrt{\sigma}$, using values of the string tension, $a^2\sigma$, obtained at the same values of β . The leading lattice correction should be $O(a^2)$ and so if we plot our values of $m/\sqrt{\sigma}$ against $a^2\sigma$, as in Fig. 10, then we can extrapolate linearly to $a = 0$ for sufficiently small a . Such extrapolations are shown in Fig. 10 and the resulting continuum values of the glueball masses are given in Table 6.

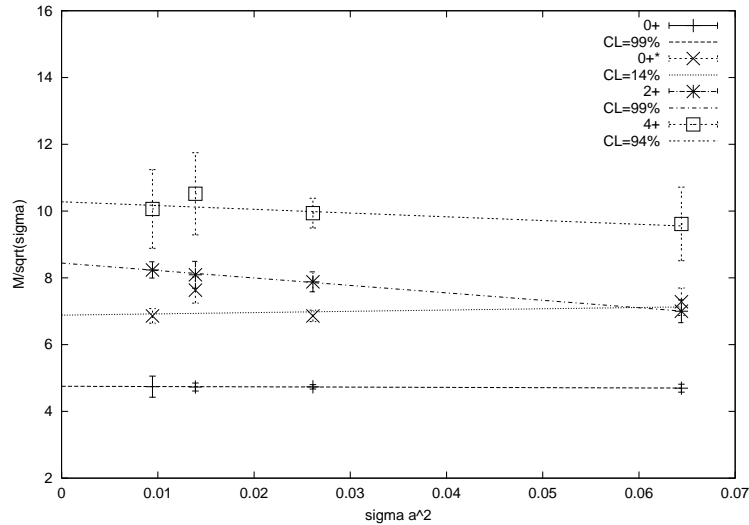


Figure 10: Strategy I: continuum extrapolation of the $J^P = (2n)^+$ masses

We note that we obtain the expected parity-degeneracies in the continuum limit for the $J = 2$ and $J = 4$ spins that we consider. We also observe that the corrections to the 4^+ mass are reasonably well fitted by a simple a^2 term for $\beta \geq 9$, just as they are for the 0^+ and 2^+ .

5 Applications of Strategy II

In this section we apply the second strategy introduced in Section 3.2 in which we probe glueball wave-functions with variously rotated operators so as to directly extract the coefficients of the Fourier modes contributing to the angular variation of those wavefunctions.

As an illustration we first apply the method to a case where we believe we know the answer, i.e. the lightest states in the A_1 and A_3 representations. We confirm that these states are indeed $J = 0$ and $J = 2$ respectively. We then return to the $0^- / 4^-$ puzzle. We establish that the lightest state in the A_2 representation is indeed spin 4 and that this is much lighter than the 0^- ground state. The evidence is more convincing than before not only because of the greater transparency of this approach, but also because we repeat the calculation closer to the continuum limit. We then go on to investigate the angular behaviour of the lightest states falling in the two-dimensional E representation which contains all of the continuum odd-spin states. Our conclusion will be that the lightest states have quantum numbers 3^\pm , rather than 1^\pm . Finally, we reanalyse the spectrum of states in the A_1 representation, and perform a continuum extrapolation, obtaining results that are consistent with those that we obtained earlier using our first method.

5.1 Wave functions of the lightest A_1 and A_3 states

To analyse the angular content of the lightest states lying in the A_1 and A_3 representations we use the four operators in Fig. (8) together with their twelve rotations. We first use the exact lattice symmetries to form operators in each of these lattice representations, and then we use the variational method to determine what are the linear combinations of these operators that provide the best approximations to the ground state glueball wavefunctionals. We then construct the same linear combinations of (approximately) the same operators rotated by different angles. This provides us with rotated versions of the ground state wavefunctionals. From the correlation at (typically) two lattice spacings between the original and rotated copies of our ground state wavefunctional, we can extract the angular variation, as displayed in Fig. (11).

We clearly observe the characteristic features of 0^+ and 2^+ wave functions. (The A_1 representation of the second operator varies more with the angle ϕ than the others. We had already noted that its correlation matrix was far from being Toeplitz and the selection criteria in Section 4.2.1 had led us to remove it from the analysis.) This provides a simple illustration of the method in a non-controversial context.

5.2 The $0^- / 4^-$ puzzle revisited

We now proceed to analyse the angular variation of the wave function of the ground state A_2 glueball on our 16^3 lattice at $\beta = 6$. We begin with the first set of operators of Section 4.1, as displayed in Fig. 5. We obtain the following mass (effective, at 1 lattice spacing) and mode decomposition (at 2 lattice spacings):

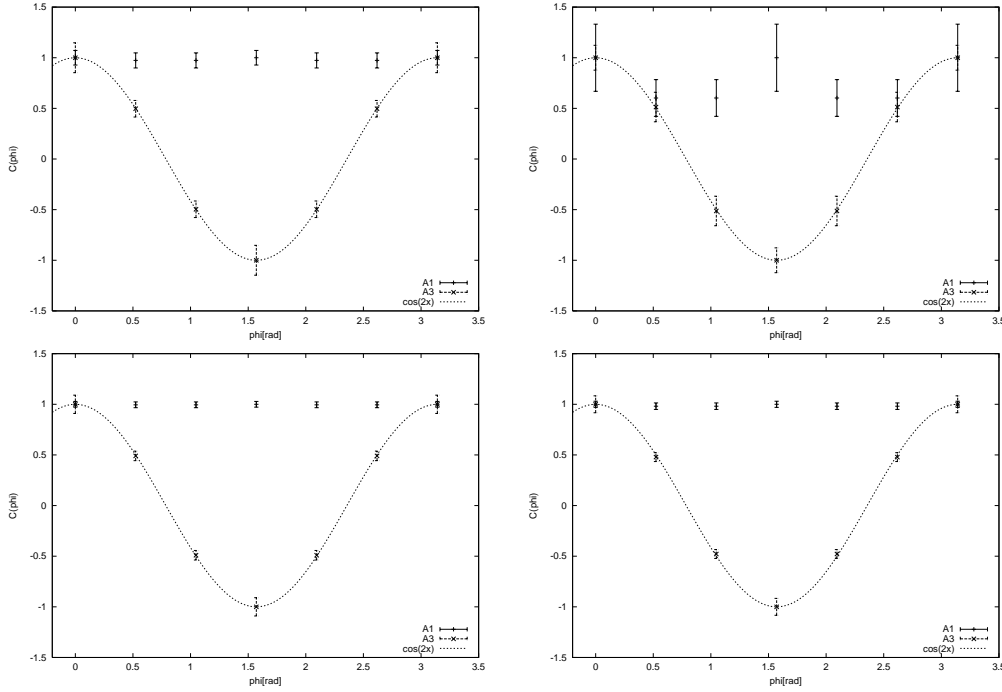


Figure 11: The wave function of the lightest state in the A_1 and A_3 lattice representations, as measured with our four operators at $\beta = 6$. The plots can be compared to the correlation matrices given in section (4.2.1).

$\beta = 6$	am	c_0	c_4
4^-	2.575(71)	-0.0525(60)	0.9986(53)

The fit, with two parameters, is to three independent points and possesses a goodness of fit given by $\chi^2 = 2.28$ (see Fig. (13)). With the second set of operators of Section 4.1 (which are rotated by $\frac{\pi}{4}$ angles, Fig. 6), we obtain the following mass and wave function (at one lattice spacing):

$\beta = 6$	am	c_0	c_4
4^-	2.455(60)	-0.224(71)	0.975(71)

The coefficients clearly show that the lightest A_2 state wave function is completely dominated by the spin 4 Fourier component. Thus, we can conclude that the 4^- ground state is lighter than the 0^- . Of course this statement holds at $\beta = 6$ and one needs to check that it is robust against lattice spacing corrections. This we now do by performing a calculation at $\beta = 12$ on a 32^3 lattice.

In principle we could proceed as before: constructing the A_2 square representation and looking at the 2-lattice-spacing correlations with an operator oriented in different directions. If we saw a $\sin(4x)$ behaviour then we could conclude that the lightest state of the A_2 representation does indeed become a 4^- state in the continuum. On the other hand, if the result was independent of the direction, then this would mean that the lightest state of the A_2 representation is a 0^- state at this β ; and probably also in the continuum limit. However there is an interesting subtlety associated with the 0^- state and the unfamiliar parity operation which

we can exploit so as to proceed somewhat differently. In $3 + 1$ dimensions, where parity commutes with all rotations, it is impossible to construct a $P = -1$ operator with Wilson loops that are $P = +1$. In general this restriction does not exist in $2 + 1$ dimensions, and we have made use of this fact when using operators that have a symmetry axis in order to obtain the masses of $P = -1$ states. However, it does apply to the spin 0 sector, where parity commutes with rotations: in other words, a linear combination of symmetric operators corresponding to the quantum numbers of the A_2 representation does not couple to the 0^- component of the lattice states. The reason is that the image of a symmetric operator under an axis-symmetry can also be obtained by a rotation, so that the relative minus sign cancels the contribution of any 0^- component. Thus we can measure the projection of the wave function onto the space orthogonal to the 0^- subspace. If the overlap onto the state whose mass we extract with this operator is not dramatically decreasing as we approach the continuum limit, we can safely conclude that the state has quantum numbers 4^- .

The kind of operators we used are triangular, as drawn in Fig.12. The corresponding wave function shown in Fig.13, confirms the last paragraph's conclusions: the data points fall perfectly on a $\sin 4x$ type curve. This result has been obtained with all the operators we employed. From the fact that our overlaps onto the state at each of $\beta = 9, 12, 14.5$ are better than 90%, we confidently conclude that the state carries quantum numbers 4^- in the continuum limit. As expected from parity doubling, it is found to be degenerate with the lightest 4^+ glueball, with a mass of $am(4^-, \beta = 12) = 1.365(56)$.

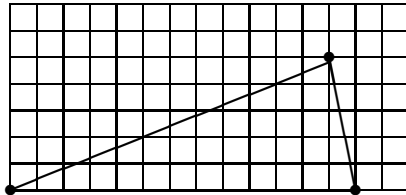


Figure 12: The triangular operator rotated by $\frac{\pi}{8}$ angles used to determine the lightest A_2 state wave function at $\beta = 12$

5.3 Wave functions of the lightest E states

Proceeding as above, we extract the angular wave function of the lightest states lying in the E representation at $\beta = 12$ (Fig. (14)). These are obtained from correlations separated by 2 lattice spacings, so as to allow the excited modes to decay relative to the contribution from the lightest states. This representation contains the continuum spin 1 and 3 states, both in the positive and negative parity channels. We clearly observe the characteristic behaviour of a spin 3 wave function. More quantitatively, the 3^+ wave function is well fitted by $0.1880(83) \cos 3\phi$ ($\chi^2 = 0.291/3$) and the 3^- by $(0.957(38) \sin 3\phi$, $\chi^2 = 0.285/3$). From this we conclude that the spin 3 glueball is lighter than the spin 1.

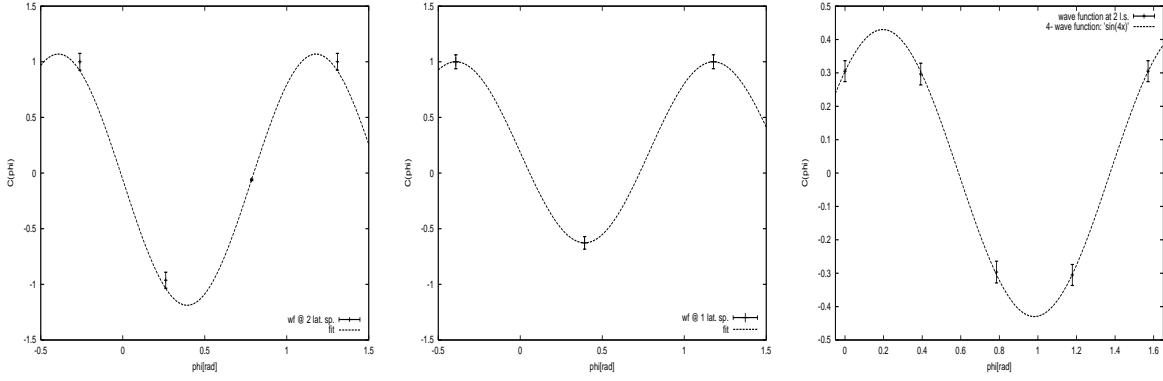


Figure 13: The wave function of the lightest state in the A_2 lattice representation; left, at $\beta = 6$ and measured with 12-fold operators ; centre, at $\beta = 6$ with 8-fold operators; right, at $\beta = 12$ with 16-fold operators. The vertical axis has arbitrary scale.

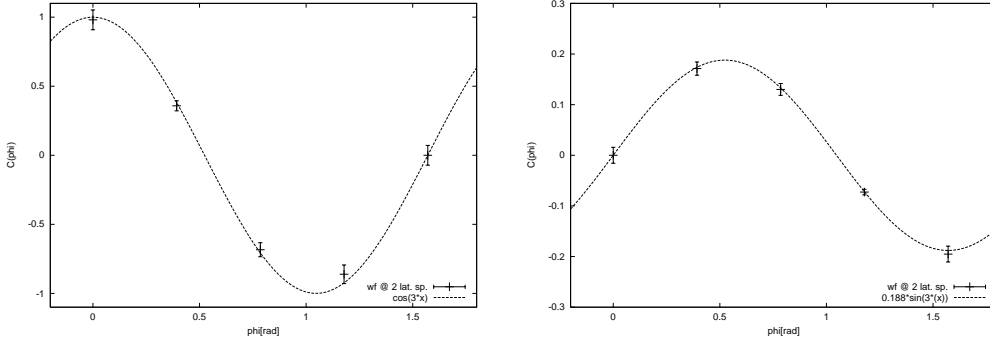


Figure 14: The wave functions of the two lightest states in the two-dimensional lattice representation E , as measured at $\beta = 12$.

5.4 The masses and Fourier coefficients in the continuum limit

Having identified at various values of β the states corresponding to different continuum spins, we can extrapolate them to the continuum limit in the usual way. This is shown in Fig.15. The masses agree with the calculations performed earlier using our “strategy I”. In identifying the lattice states as belonging to particular continuum spins, we assume that the appropriate Fourier coefficient $|c_n|^2$ will extrapolate to unity in the continuum limit. A check that this is so is provided in Fig.16 where we show an extrapolation of the 4^+ component of the A_1^{**} state, as well as the 0^+ component of the A_1^{**} state. Although the error bars are relatively large, the data allows use to draw definite conclusions about the quantum number of these states in the continuum.

6 Generalisation to (3+1) dimensions

We note that the ideas on high spin wave functions described for simplicity in the plane carry over directly to three dimensions. The wave functions are now spherical harmonics; the $D^{(j)m}_{m'}(\alpha, \beta, \gamma)$ matrices tell us how they transform under rotations. Here (α, β, γ) are Euler

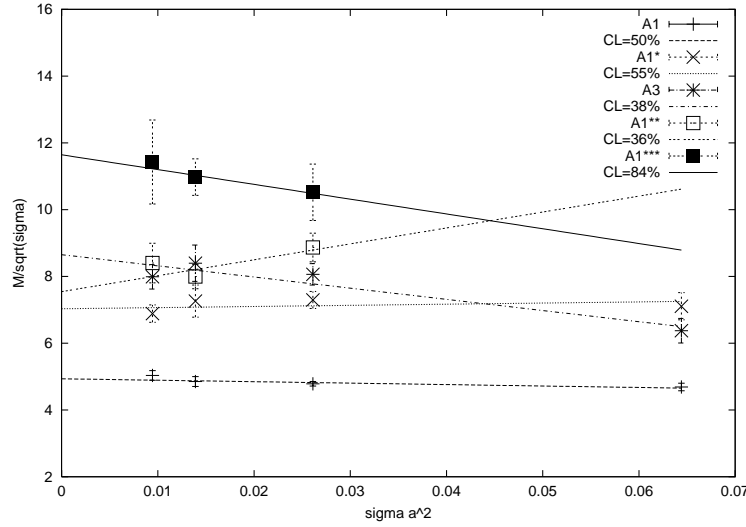


Figure 15: Continuum extrapolation of the $J^P = (2n)^+$ masses, as obtained with strategy II

angles. Recall that the point of this parametrisation is that

$$R(\alpha, \beta, \gamma) \equiv R_{z''}(\alpha) R_{y'}(\beta) R_z(\gamma) = R_z(\gamma) R_{y'}(\beta) R_z(\alpha) \quad (24)$$

where indexes indicate the axis of rotation and the argument the angle. A prime denotes the image of an axis under the preceding rotation in the definition of $R(\alpha, \beta, \gamma)$. The nice feature of the second expression for R is that it contains only rotations around the Cartesian axes, making it very easy to compute. Now, by definition, $D^{(j)m}_{m'}$ is a representation of the rotation group:

$$U(\alpha, \beta, \gamma)|j, m\rangle = \sum_{m'} D^{(j)m}_{m'}(\alpha, \beta, \gamma)|j, m'\rangle \quad (25)$$

so that the 3-dimensional equivalent of (2) reads

$$\mathcal{O}_{j,m}^{(m')} \propto \int d\gamma d(\cos \beta) d\alpha D^{(j)m}_{m'}(\alpha, \beta, \gamma) \mathcal{O}(\alpha, \beta, \gamma) \quad (26)$$

where $\mathcal{O}(\alpha, \beta, \gamma)$ represents an operator rotated in the direction (α, β, γ) . Thus, if we want to measure the mass of a state $|j, m\rangle$, there is a choice for $m' \in \{-j, \dots, j\}$. Although a general expression exists for D , in order to construct a (j, m) operator it is sufficient to know the following property:

$$D^{(j)m'}_m(\alpha, \beta, \gamma) = e^{-i\alpha m'} d^{(j)}(\beta)_m^{m'} e^{-i\gamma m} \quad (27)$$

with

$$d^{(j)}(\beta)_0^m = \left(\frac{(j-m)!}{(j+m)!} \right)^{\frac{1}{2}} P_j^m(\cos \beta) \quad (28)$$

Here $P_j^m(z)$ is a Legendre function. Thus a simpler, yet general enough version of (26) is

$$\mathcal{O}_{j,m} \equiv \mathcal{O}_{j,m}^0 = \int d\gamma d(\cos \beta) d\alpha P_j^m(\cos \beta) e^{im\gamma} \mathcal{O}(\alpha, \beta, \gamma) \quad (29)$$

The higher complexity of these wave functions will make it more difficult to project out states with a discretised approximation to (29) of the kind used in our strategy I. For that reason we

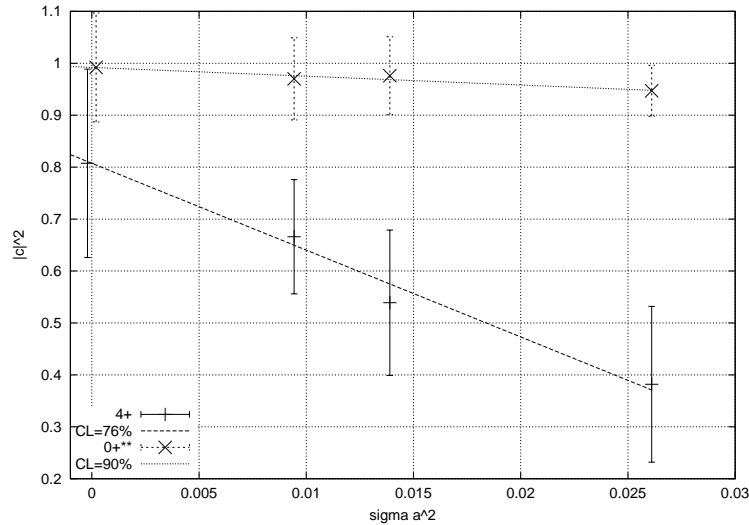


Figure 16: Continuum extrapolation of coefficient c_0 for the A_1^{**} state and coefficient c_4 for the A_1^{***} state. The continuum values are 0.996(53) and 0.81(18) respectively. Thus the former state evolves to a 0^+ , the latter a 4^+ state in the continuum limit.

expect the second strategy, where the wave function information is extracted from the lattice rather than being assumed, to become our main method. The $2j + 1$ degeneracy of states (in the continuum limit) should provide us with a powerful consistency check.

7 Previous work

There have been two recent calculations of the 4^+ glueball mass in D=2+1 SU(2) gauge theories [15,17], and a calculation of the 4^{++} glueball mass in the D=3+1 SU(3) gauge theory [16]. We shall now briefly comment upon these earlier calculations.

The calculation in [15] starts with rectangular Wilson loops constructed out of simple, blocked link matrices and constructs other Wilson loops that are approximate $\pi/4$ rotations of these. Linear combinations of these are taken to produce, altogether, twelve trial 0^+ and 4^+ operators. The overlaps at $t = 0$ of corresponding $J = 0$ and $J = 4$ operators are calculated and operators with substantial overlaps are discarded. This leaves nine pairs of operators with smaller overlaps. Effective masses at $t = a$ are obtained from the diagonal correlators of these nine pairs of operators, and the minimum effective mass in each set provides an estimate of the lightest glueball of the appropriate spin. The calculation is at $\beta = 9$ on a $L = 24$ lattice and the estimate of the lightest $J = 4$ glueball mass, $am(J = 4) = 1.607(27)$, is consistent with the estimates in the present paper at that value of β . However the method is very similar to the naive precursor of our Strategy I, which served as a caveat in Section 3.3. No attempt is made to determine if the ‘J=4’ state is not in fact an excited $J = 0$ state and no approach to the continuum is attempted. That is to say, the control over the relevant systematic errors is almost entirely lacking.

The calculation in [17] is similar to that in [15] except that it uses the matrix method described in Section 2.1 to construct the ‘sides’ of suitably chosen Wilson loops. These involve (approximate) copies rotated by angles that are multiples of $\pi/3$. Such Wilson loops are allowed to come in four different sizes and calculations are performed with the parameter α

in eqn(6) taking values $\alpha = 0.1, 0.15, 0.2, 0.25$. (There is no smearing of the link matrices that enter as the elements of the original matrix.) Taking suitable linear combinations one thus obtains sixteen trial 0^+ and 4^+ operators. The overlaps at $t = 0$ of corresponding $J = 0$ and $J = 4$ operators are calculated and the operator for which the overlap is minimal (and indeed negligible) is used to extract a $J = 4$ mass estimate from the diagonal correlator at $t = a$. The calculation is on a $L = 16$ lattice at $\beta = 6$. The operator corresponds to the largest loop and $\alpha = 0.2$. Using eqn(11) such a value of α translates into a scalar propagator mass of about $am_0 \simeq 1.0 \simeq 4a\sqrt{\sigma}$ which is rather large and would suggest that the effective smearing is weak. The $t = a$ mass estimate for the 4^+ glueball is $am(J = 4) = 2.13(4)$ which is significantly lower than our $\beta = 6$ mass estimate. Also puzzling is the fact that some of the $t = a$ 2^+ glueball effective masses are significantly lower than the usually accepted mass estimate for this supposedly uncontroversial state. In any case, this calculation suffers from a poor control over most of the systematic errors that we listed earlier in discussing the calculation of [15].

The calculation in [16] is in D=3+1 so we cannot, for the moment, compare their results with ours. Their approach is to expand small Wilson loops in terms of continuum fields and their covariant derivatives so as to identify a linear combination that is $J = 4$. Such a linear combination is then used as a 4^+ trial operator. The calculations are performed for very coarse spatial lattice spacings, presumably because only there can small unsmearred Wilson loops act as useful glueball wavefunctionals. However for such coarse spatial lattice spacings one might worry about the relevance of the continuum field expansion that motivates the spin assignment. On the positive side, an improved action is used which one might hope would reduce any lattice corrections. A continuum extrapolation is performed, albeit over a range of spatial lattice spacings that are large. It would certainly be worthwhile to pursue this interesting method further incorporating some of the checks described in our paper.

8 Conclusions

To calculate the mass of a glueball of spin J in a lattice calculation, one must identify the lattice energy eigenstate that tends to that state in the continuum limit. The limited rotational invariance on a lattice introduces ambiguities which means that at a fixed value of a one cannot be confident in one's spin assignment. Only by performing a continuum extrapolation while monitoring the angular content of the glueball wavefunctional, can one be confident in the mass one extracts for a high spin glueball.

In practise one needs to identify likely candidates for such lattice eigenstates and we introduced two related strategies to do so. The first tries to construct wavefunctionals with the required rotational symmetry, which of course can only be approximate at finite a . The second probes the angular variation of eigenstates obtained through a conventional lattice calculation, using probes that have the required rotational symmetry, which again can only be approximate at finite a . In either case one needs to be able to easily calculate smeared Wilson loops with arbitrary shapes, and we developed methods for doing so.

To test our methods we applied them to the relatively simple problem of determining whether the 4^- is lighter than the 0^- in D=2+1 gauge theories. The physical interest of this possibility lies in the fact that it is predicted by flux loop models of glueballs and it is plausible that such models are relevant to glueball structure in D=3+1. Our calculations confirmed unambiguously that the ground state 4^- glueball is indeed much lighter than the ground state 0^- glueball, so that the usual identification of the ground state of the A_2 representation as

being 0^- is mistaken. Similarly we showed that the 4^+ state degenerate with this 4^- is usually misidentified as the 0^{+***} . (It is of course possible that with a larger basis of operators we would resolve additional excitations of the 0^+ that are lighter than the 4^+ .)

In applying our methods we found that the second strategy was in practise the more transparent and reliable. Although it is more affected by the mixing that occurs if two levels that correspond to different (continuum) spins cross as we reduce a , such crossings should be easy to spot and to take into account.

Our calculations make us confident that calculating higher spin glueball masses is a practical task. Currently we are extending our work to a full continuum extrapolation covering the range $\beta = 9$ to 18 and extending to higher spins than four [25]. This will enable us to see if the glueball mass spectrum defines a ‘Pomeron’ trajectory in two space dimensions. At the moment our calculations are for $SU(2)$ but it is plausible that the simplicity of a linear Pomeron trajectory will only become manifest in the $SU(N \rightarrow \infty)$ theory and we hope to explore that limit as well. Of course the question of real physical interest is whether glueballs define the Pomeron(s) in $D=3+1$ with the $SU(3)$ gauge group of the strong interactions. As we pointed out, the general ideas, applied here for simplicity in the plane, carry over directly to three dimensions, where the wave functions are spherical harmonics and the $2j + 1$ degeneracy of states provides a useful consistency check in the determination of the continuum spectrum. We are currently performing calculations of higher spin glueballs in the $D=3+1$ $SU(3)$ gauge theory at intermediate lattice spacings.

Acknowledgements.- One of us (HM) thanks the Berrow Trust for financial support.

References

1. T. H. Hansson, in *Non-perturbative Methods* (Ed. S. Narison, World Scientific 1985)
2. N. Isgur and J. Paton, Phys. Rev. D31 (1985) 2910.
3. T. Moretto, M. Teper, hep-lat/9312035.
4. R. Johnson, M. Teper, Nucl. Phys. Proc. Suppl. 63 (1998) 197 (hep-lat/9709083).
5. G. Karl and J. Paton, Phys. Rev. D61 (2000) 074002 (hep-ph/9910413).
6. R. Johnson, M. Teper, Phys. Rev. D66 (2002) 036006 (hep-ph/0012287).
7. P. Landshoff, hep-ph/0108156.
A. Kaidalov, hep-ph/0103011.
8. M. Teper, Invited Talk at the John Hopkins Workshop 2002.
9. M. Teper, Phys. Rev. D59 (1999) 014512 (hep-lat/9804008).
10. M. Lüscher, U. Wolff, Nucl. Phys. B339 (1990) 222.
11. M. Teper, Nucl. Phys. Proc. Suppl. 4 (1988) 41 and unpublished.
12. Lang, C. Rebbi, Phys. Lett. B115(1982) 137
13. Ph. de Forcrand, G. Schierholz, H. Schneider, M. Teper, Z. Phys. C31(1986) 87
14. C. Morningstar, M. Peardon, Phys. Rev. D60:034509, 1999
15. R. Johnson, M. Teper, Nucl. Phys. Proc. Suppl. 73 (1999) 267 (hep-lat/9808012).
16. Da Qing Liu, Ji Min Wu, Mod.Phys.Lett. A17 (2002) (hep-lat/0105019).
17. R. Johnson, D.Phil. thesis, Oxford University, 2001 and hep-lat/0206005.
18. J. Smit, *Introduction to Quantum Fields on a Lattice*, Cambridge 2002.
H. Rothe, *Lattice Gauge Theories* 2nd Edition, World Scientific 1997.
I. Montvay and G. Munster, *Quantum Fields on a Lattice*, Cambridge 1994.
M. Creutz, *Quarks, gluons and lattices*, Cambridge 1983.
19. T. Banks and A. Casher, Nucl. Phys. B169 (1980) 103.
20. M. Teper, Phys. Lett. B183 (1987) 345.
21. M. Albenese et al (APE Collaboration), Phys. Lett. B192 (1987) 163.
22. N. Cabibbo and E. Marinari, Phys. Lett. B 119 (1982) 387.
23. Kennedy, Pendleton, Phys. Lett., 156B (1985) 393.
24. S.L. Adler, Phys. Rev. D 23 (1981) 2901.
25. H. Meyer, M.J. Teper, in preparation.

A Properties of the M matrix

Basic properties

$$\begin{aligned}\text{Tr}M^{2n+1} &= \sum_i \lambda_i^{2n+1} = 0 \quad \forall n \\ \text{Tr}M^2 &= \sum_i \lambda_i^2 = 4n^2 \quad \Rightarrow \quad \sqrt{\langle \lambda^2 \rangle} = 2 \\ \text{Tr}M^4 &= \sum_i \lambda_i^4 = 4 \sum_i \text{Tr}P_i + 32n^2 \quad \Rightarrow \quad \langle \lambda^4 \rangle = 4\langle P \rangle + 32\end{aligned}$$

The frozen configuration

The spectrum of the matrix M in the frozen configuration (all links set to 1) is the following:

$$\lambda_{ab} = 2 \left(\cos\left(\frac{2\pi a}{L}\right) + \cos\left(\frac{2\pi b}{L}\right) \right) = 4 \cos\left(\frac{2\pi(a+b)}{L}\right) \cos\left(\frac{2\pi(a-b)}{L}\right), \quad a, b = 1, 2, \dots, L \quad (30)$$

with corresponding eigenvectors

$$v_{ab} = \left(1, \lambda_a, \lambda_a^2, \dots, \lambda_a^{L-1}, \lambda_b, \lambda_b \lambda_a, \dots, \lambda_b \lambda_a^{L-1}, \dots, \lambda_b^{L-1}, \lambda_b^{L-1} \lambda_a, \dots, \lambda_b^{L-1} \lambda_a^{L-1} \right) \quad (31)$$

where

$$\lambda_a = \exp\left(\frac{2\pi i a}{L}\right). \quad (32)$$

The $(\ell = 2k + m + n)^{th}$ power of M reads:

$$M^{2k+m+n}[m, n] = \binom{2k+m+n}{k+n} \binom{2k+m+n}{k}, \quad k \geq 0 \quad (33)$$

and of course $M^{m+n+2k+1}[m, n] = 0, \forall k$. Thus the expression of the superlink from point $x(0, 0)$ to $y(m, n)$ reads:

$$K[m, n] = \sum_{k \geq 0} \binom{2k+m+n}{k+n} \binom{2k+m+n}{k} \alpha^{2k+m+n} \quad (34)$$

Asymptotically, the binomial coefficients tend to

$$\binom{2k}{k} \sim \frac{4^k}{\sqrt{k}}, \quad k \rightarrow \infty, \quad (35)$$

so that $K[m, n]$ becomes singular at $\alpha = \frac{1}{4}$ for any (m, n) . This is as expected from the spectrum of M , the maximum of which is 4, and corresponds to our test-charge becoming massless. We will be mainly interested in the case where α is close to its critical value. However one must realise that this is the opposite limit of that in which the quenched approximation would become valid, namely $m \rightarrow \infty$. Therefore K is far away from the propagator of the physical (unquenched) theory mentioned above.

The decay rate of the terms in (34) the series is easily found: since the terms behave like $(16\alpha^2)^k$, the correlation length is

$$\frac{\xi_\ell}{a} = \frac{-1}{\log(4\alpha)} \quad (36)$$

As $\alpha \rightarrow \frac{1}{4}$, the correlation length diverges logarithmically in α . It might seem surprising that we have already seen another distance scale related to α , namely the inverse mass of the scalar particle whose propagator is precisely K . But that correlation length ξ_d was related to the distance the test-charge can propagate, while here $\xi_\ell = \ell - d$, where ℓ is the length of the typical path the particle takes to propagate from $(0, 0)$ to $(0, d)$:

$$am_\ell = \log \left(1 + \left(\frac{am_d}{2} \right)^2 \right) \quad (37)$$

When am_d goes to zero, we have to leading order

$$am_\ell \simeq \left(\frac{am_d}{2} \right)^2 \quad (38)$$

That is, in terms of correlation lengths in lattice units,

$$\frac{\xi_d}{a} = \frac{1}{2} \sqrt{\frac{\xi_\ell}{a}}, \quad \alpha \rightarrow 0 \quad (39)$$

This is precisely the behaviour of a *Brownian motion*: the distance by which the particle is displaced after a path of length ℓ is asymptotically proportional to the square root of ℓ^4 . The limit $am_d \rightarrow 0$ can also be interpreted as the continuum limit. Thus we have in fact established the connection between the Brownian propagation of the test charge and the continuum limit. Since rotation invariance is only regained in the continuum limit, we now know that *it is only when our test-charge is following random walks that rotation invariance is restored*.

When on the other hand $\alpha \rightarrow 0$, $\xi_d \rightarrow 0$ and therefore also $\xi_\ell \rightarrow 0$, so that the length of the typical path taken by the test-charge to move from $(0, 0)$ to $(d, 0)$ is simply d . Therefore, the exponent η defined by

$$\eta(d) = \frac{\log \bar{\ell}(d)}{\log d} \quad (40)$$

should always take values between 1 and 2; the first extreme value corresponds to a completely directed motion, the second to a random walk. As α is increased from 0 to $\frac{1}{4}$, we expect to cross over from the first to the second regime.

One has to be careful about the range of validity of this analysis. The conclusions are based on the idea that the dominant contribution to the propagator comes from the long paths governed by an exponential law with correlation length ξ_ℓ . But this only holds for distances d smaller than ξ_d . For propagation over larger distances, following a path of length $\ell = d + \Delta\ell$ is suppressed, not by $e^{-am_\ell \Delta\ell}$, but by $e^{-am_d \Delta\ell}$, which is a much stronger suppression in view of (38). Therefore, for $d \gg \xi_d$, the scale ξ_ℓ becomes irrelevant and we have a directed type of motion, *however close to the critical point we are*. Since, as we have seen, d can only be neglected in the propagation law $\bar{\ell} = d + 4d^2$ if $d \gg 1$, *the brownian motion regime only holds for distances*

$$1 \ll d \ll \xi_d \quad (41)$$

Thus, for $[1, \xi_d]$ to be a non-zero interval, we must work with $\alpha > \frac{1}{5}$, otherwise the Brownian motion regime does not exist on any length scale at all.

⁴Another consequence of this result is that if one maintains d fixed in physical units as one takes the continuum limit, then the different scaling properties of ξ_d and ξ_ℓ imply that ξ_ℓ diverges like a^{-1}

Illustration

To show to which power of 'd' ℓ is proportional to asymptotically, we plot $\eta \equiv \frac{\log \ell_{max}(d)}{\log d}$ as a function of d in Fig. (17), for several values of α . The variable η represents the local power law:

$$\ell_{max}(d) \propto d^\eta. \quad (42)$$

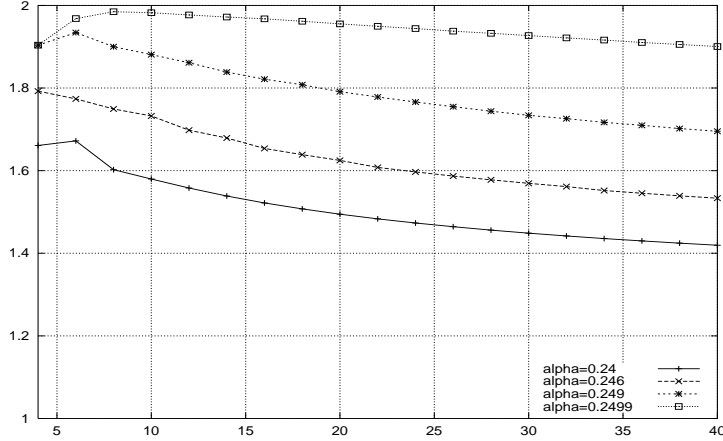


Figure 17: $\eta \equiv \frac{\log \ell_{max}(d)}{\log d}$ as a function of d

We observe that all exponents lie between 1 and 2, and are closer to 2. Inverting eqt. (42), we see that $\eta \simeq 2$ corresponds to $d \sim \sqrt{\ell}$. This is precisely the scaling law of the distance d covered in a random walk in a time ℓ . On the other hand, $\eta \simeq 1$ expresses that the paths are well orientated towards the final point $(d, 0)$. Because of this interpretation, we may consider η as an “order parameter”. The plot illustrates that *the closer α is to its critical value, the more the propagation resembles a Brownian motion.*

Rotation invariance test In the long-path limit, $r \equiv \sqrt{m^2 + n^2} \rightarrow \infty$, we expect to obtain rotational invariance, in the sense that $K(x, y)$ is constant at fixed r . One easy way to check this is to choose Pythagorean numbers (a, b, c) , such as $(3, 4, 5)$, $(5, 12, 13)$, $(7, 24, 25)$, for which $a^2 = b^2 + c^2$, and to compare $K(\lambda a, \lambda b)$ to $K(\lambda c, 0)$. This is illustrated on Fig. (18), where the relative difference

$$\Delta \equiv \frac{2 \left(K(\lambda, 0) - K\left(\frac{3}{5}\lambda, \frac{4}{5}\lambda\right) \right)}{K(\lambda, 0) + K\left(\frac{3}{5}\lambda, \frac{4}{5}\lambda\right)} \quad (43)$$

is plotted as function of λ for different values of α .

At a fixed size λ , the relative difference decreases when $\alpha \rightarrow \frac{1}{4}$. This is as expected from the preceding analysis, which showed that close to the critical behaviour, propagation can be thought of as a Brownian motion, which means that the dominantly contributing paths are much longer than λ . In the “long-path dominance” limit, it is expected that rotational invariance, since any continuum path can be accurately approximated by a lattice path, as one would do to evaluate a path integral numerically.

At a fixed value of α , and varying λ , the situation is more complicated: at first, for all the considered α , the difference decreases with the length of the superlinks. But we observe

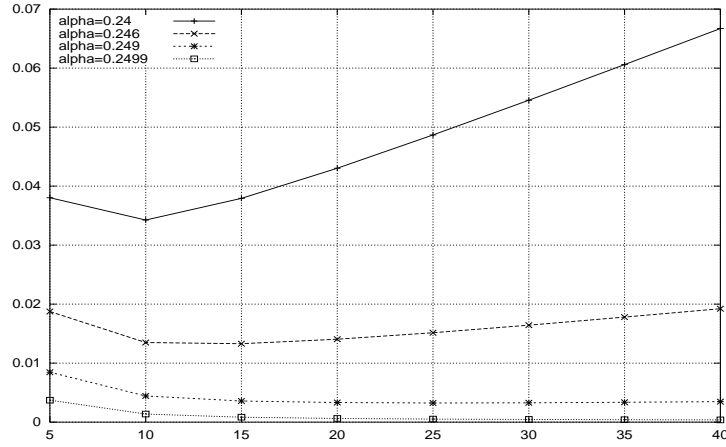


Figure 18: $\frac{2(K(\lambda,0)-K(\frac{3}{5}\lambda,\frac{4}{5}\lambda))}{(K(\lambda,0)+K(\frac{3}{5}\lambda,\frac{4}{5}\lambda))}$ as function of λ , for several values of α

that $\forall \alpha$, the difference ultimately increases at large λ . The physical interpretation is that for λ large, the paths have a very accurately defined direction in which to move, and however small $|\alpha - \frac{1}{4}|$, λ always becomes larger than the finite size of the “cloud” of paths. Therefore the propagation becomes directional, and we end up in the regime where $\ell_{max} \propto d$, as we saw above in a more analytical way⁵

Finite volume effects We have seen that extremely long paths can contribute to the superlinks. When working on a finite lattice with periodic boundary conditions, paths can easily go “around the world”. On a torus, the length of such paths is greater if done along a diagonal than along a lattice axis. Could that spoil our conclusions on the rotational invariance of K ? We illustrate in Fig. (19) how the finite volume affects the quantity Δ .

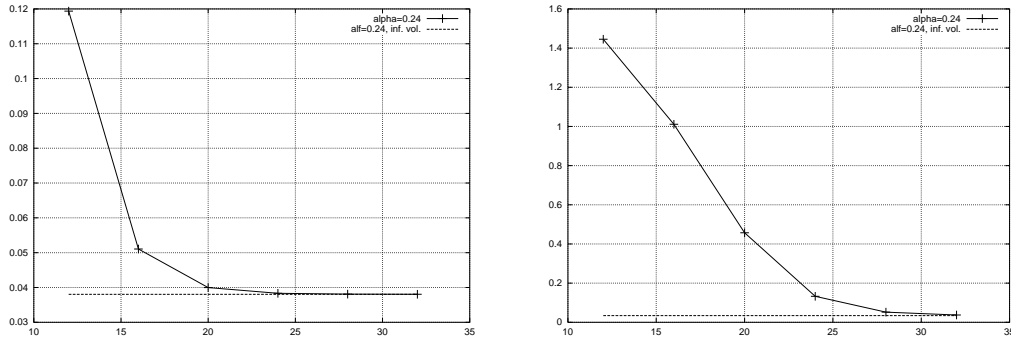


Figure 19: Δ as function of the lattice size L , for the couple of links a) (3,4) and (5,0), at $\alpha = 0.24$ and b) (6,8) and (10,0); the asymptotic value for infinite volume is indicated as a constant

Due to “paths around the world”, significant finite volume effects are seen when looking

⁵These conclusions are the consequence of the fact that (34) for $(m,n) = (d,0)$ is an asymptotic series in d .

at the difference between superlinks of same Euclidean length, pointing in different directions.

Spectrum of the M matrix It is useful to know how the spectrum of the M matrix in a finite β configuration differs from the frozen configuration spectrum. Fig. (20) shows the spectrum of M on a 16^2 lattice both in the frozen configuration and at $\beta = 6$. For individual Monte-Carlo generated gauge field configurations, the spectrum of the frozen configuration gets smeared out by statistical fluctuations. Its qualitative features do not vary much with β or L at values that are customary in simulations. The maximum of the spectrum is in 90% of cases situated between 4 and 4.1. Therefore a large enough, yet safe value of α to work with is 0.24.

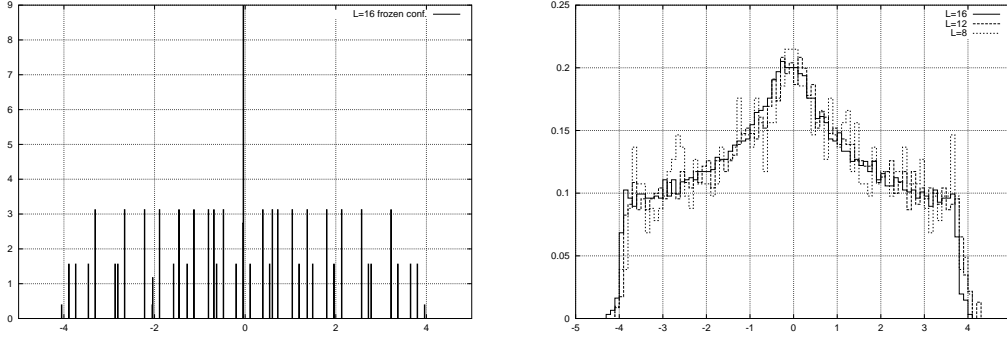


Figure 20: The eigenvalues of the M matrix a) on a frozen 16^2 lattice b) at $\beta = 6$ and different lattice sizes

B Parity and rotations in continuous (2+1) dimensions

The rotation group $SO(2)$ being abelian, its irreducible representations are one-dimensional:

$$\langle \phi | j \rangle = e^{ij\phi}$$

Here j takes all positive and negative values.

The parity transformation, i.e. a flip around an axis, takes a clockwise-winding state into an anticlockwise-winding state, so that

$$P|j\rangle = e^{i\theta}|-j\rangle,$$

which implies that P and J do not commute and therefore cannot be diagonalised simultaneously. For a particular choice of axis, θ can be chosen to be zero. The fact that the Hamiltonian is parity-invariant implies that the $|j\rangle$ and $|-j\rangle$ are degenerate:

$$E_j = \langle j | H | j \rangle = \langle Pj | PHP | Pj \rangle = \langle -j | H | -j \rangle = E_{-j} .$$

This fact is called “parity doubling”.

It is also straightforward to show that

$$\{J, P\} = 0.$$

As a consequence, 'parity' as defined with an axis rotated by an angle ϕ with respect to the reference axis will be related to P according to

$$P_\phi \equiv e^{iJ\phi} P e^{-iJ\phi} = e^{2iJ\phi} P = P e^{-2iJ\phi}$$

In particular, acting on a spin $j \neq 0$, this relation implies that

$$P_\phi |j\rangle = -P |j\rangle, \quad \phi = \frac{\pi}{2j}$$

Thus an elegant way to understand parity doubling is that the $P = \pm 1$ labelling can be reversed by the use of another convention; except for the spin 0, where all choices of parity axis will label the states in the same way.

C Irreducible representations of the square group

The character table of the symmetry group of a 2-dimensional time-slice is given below. C_4 are the rotations by $\frac{\pi}{2}$, C_2 is the rotation by π , σ is the reflexion around the x axis, σ' is the reflexion around the $y = x$ axis.

fct.		E	$2C_4$	C_2	2σ	$2\sigma'$
1	$(0^+, 4^+, \dots) \rightarrow A_1$	1	1	1	1	1
$xy(x^2 - y^2)$	$(0^-, 4^-, \dots) \rightarrow A_2$	1	1	1	-1	-1
$x^2 - y^2$	$(2^+, 6^+, \dots) \rightarrow A_3$	1	-1	1	1	-1
xy	$(2^-, 6^-, \dots) \rightarrow A_4$	1	-1	1	-1	1
(x, y)	$(1^\pm, 3^\pm, \dots) \rightarrow E$	2	0	-2	0	0
$(x + iy)^j$	D_j	2	$2 \cos \frac{j\pi}{2}$	$2 \cos j\pi$	0	0

It is interesting that 1^+ and 1^- are exactly degenerate on the lattice – they belong to the same representation on the lattice –, while the 2^- and 2^+ are not. Applying the projection rules for characters, we can immediately find how the spin J representation D_J decomposes onto the irreducible representations of the square group. For instance:

$$D_4 = A_1 \oplus A_2$$

D Irreducible representations of the cubic group

The character table of the rotation symmetry group (432) of a 3-dimensional time-slice is given below. The insertion of parity in the group ((m3m): $O_h = O \times i$) does not introduce any complications as in two dimensions, because parity commutes with rotations and is realised exactly on the lattice. C_4 are the rotations by $\frac{\pi}{2}$, C_2 by π (3 along the axes and 6 along face diagonals) and C_3 are the ternary axes along the volume diagonal.

fct.	repr.	E	$8C_3$	$3C_2$	$6C_2$	$6C_4$
1	A_1	1	1	1	1	1
$xyz \propto Y_3^2 - Y_3^{-2}$	A_2	1	1	1	-1	-1
$(Y_2^0, Y_2^2 + Y_2^{-2})$	E	2	-1	2	0	0
$(x, y, z), (Y_1^1, Y_1^{-1}, Y_1^0)$	T_1	3	0	-1	-1	1
$(Y_2^1, Y_2^{-1}, Y_2^2 - Y_2^{-2})$	T_2	3	0	-1	1	-1
Y_j^m	D_j	$2j + 1$	$(1, 0, -1)$	$(1, -1)$	$(1, -1)$	$(1, 1, -1, -1)$

In the last line, the different values of $\chi_j(C_n)$ correspond to $j \equiv 0, \dots, n-1 \pmod{n}$. These values are easily obtained from the general formula

$$\chi_j(\alpha) = \frac{\sin(j + \frac{1}{2})\alpha}{\sin \frac{\alpha}{2}}.$$

Thus the smallest spins coupling to the various lattice representations are

$$\begin{aligned} A_1 &\rightarrow \text{spin } 0 \\ T_1 &\rightarrow \text{spin } 1 \\ E &\rightarrow \text{spin } 2 \\ T_2 &\rightarrow \text{spin } 2 \\ A_2 &\rightarrow \text{spin } 3 \end{aligned}$$

Inversely, a few useful decompositions of the continuum representations read

$$\begin{aligned} D_0 &= A_1 \quad (\text{scalar}) \\ D_1 &= T_1 \quad (\text{vector}) \\ D_2 &= E \oplus T_2 \quad (\text{tensor}) \\ D_3 &= A_2 \oplus T_1 \oplus T_2 \\ D_4 &= A_1 \oplus E \oplus T_1 \oplus T_2 \\ D_5 &= E \oplus 2T_1 \oplus 2T_2 \\ D_6 &= A_1 \oplus A_2 \oplus E \oplus T_1 \oplus 2T_2 \end{aligned} \tag{44}$$

Tables

10	-3	-10	3
6	5	-6	-5
14	-4	-14	4
8	7	-8	-7
6	5	-6	-5
0	3	0	-3
8	7	-8	-7
0	4	0	-4

10	-3	-10	3
6	5	-6	-5
15	-3	-15	3
9	5	-9	-5
14	-4	14	4
8	7	-8	-7
6	5	-6	-5
0	3	0	-3
12	10	-12	-10
0	6	0	-6
8	7	-8	-7
0	4	0	-4

13	-8	-5	
0	12	-12	
13	-1	-12	
0	5	-5	
18	-1	-17	
0	7	-7	
13	12	-13	-12
0	5	0	-5
21	-6	-21	6
12	14	-12	-14
24	-5	-24	5
10	12	-10	-12

Table 1: Vector coordinates of the operators used at $\beta = 6$ (12-fold rotations; left), at $\beta = 9$ (12-fold rotations; center) and $\beta = 12/ 14.5$ (16-fold rotations; right). They are given in line, the upper/lower corresponding to the x and y components of the vector joining one point of the polygon to the next one.

$\beta = 6$	$am(t=a)$	$am(t=2a)$	quality[%]	overlap[%]
0^+	1.2309(77)	1.203(27)	97.2(36)	6.3
0^{+*}	1.995(23)	1.79(12)	81.4(12)	4.8
2^+	1.998(12)	1.777(80)	80.1(74)	4.1
2^-	1.947(11)	1.70(12)	78(10)	9.9
4^+	2.509(24)	2.44(27)	93(27)	13.8
4^-	2.536(35)	2.42(37)	89(36)	/

$\beta = 9$	$am(t=a)$	$am(t=2a)$	$am(t=3a)$	quality[%]	overlap[%]
0^+	0.8053(85)	0.7681(93)	0.739(22)	96.3(21)	6.9
0^{+*}	1.1904(82)	1.159(28)	0.995(12)	96.9(36)	5.9
2^+	1.3311(71)	1.287(47)	1.156(97)	95.6(54)	5.5
2^-	1.410(13)	1.301(49)	1.16(21)	89.7(58)	9.0
4^+	1.721(14)	1.623(66)	1.70(45)	90.7(76)	2.0
4^-	1.709(18)	1.67(11)	1.58(52)	96(12)	/

$\beta = 12$	$am(t=a)$	$am(t=2a)$	$am(t=3a)$	$am(t=4a)$	quality[%]	overlap[%]
0^+	0.6337(54)	0.5845(66)	0.567(14)	0.558(27)	91.8(41)	1.8
0^{+*}	1.054(11)	0.946(22)	0.899(47)	0.95(14)	81.6(96)	3.3
2^+	1.0991(55)	1.030(20)	0.991(54)	0.86(11)	86(11)	4.0
2^-	1.0928(71)	1.009(29)	0.946(98)	0.70(14)	81(19)	2.6
4^+	1.4105(86)	1.364(45)	1.24(14)	0.70(24)	95.5(53)	5.7
4^-	1.412(10)	1.328(50)	1.20(15)	0.95(28)	91.9(58)	/
3^+	1.611(12)	1.525(69)	2.09(63)	/	91.8(76)	7.5
1^+	1.863(25)	1.72(13)	/	/	87(14)	1.7
3^-	1.644(12)	1.680(83)	1.64(47)	/	100(10)	7.0
1^-	1.889(21)	1.79(13)	/	/	91(14)	1.8

$\beta = 14.5$	$am(t=a)$	$am(t=2a)$	$am(t=3a)$	$am(t=4a)$	quality[%]	overlap[%]
0^+	0.5823(42)	0.5107(57)	0.4921(79)	0.486(15)	79(11)	3.3
0^{+*}	0.7999(51)	0.732(11)	0.666(20)	0.601(40)	82.0(46)	8.2
2^+	0.9851(52)	0.883(12)	0.800(22)	0.786(69)	76.4(47)	1.1
2^-	0.9413(70)	0.867(12)	0.826(30)	0.822(84)	85.4(68)	3.7
4^+	1.413(13)	1.184(41)	0.98(11)	1.14(38)	91.0(26)	9.2
4^-	1.2698(91)	1.196(43)	1.028(97)	/	92.9(51)	/
3^+	1.527(26)	1.64(11)	1.66(77)	/	100(15)	2.5
3^-	1.563(16)	1.569(54)	1.73(40)	/	100(72)	2.7
1^+	1.732(20)	1.616(86)	1.65(63)	/	89.0(96)	4.4
1^-	1.68(17)	1.7(1.0)	/	/	/	3.9

Table 2: Strategy I: The local effective masses, quality factors and overlaps (as defined in the text) between states of different wave functions at $\beta = 6, 9, 12$ and 14.5 . For the 0^+ at $\beta = 14.5$, we used the effective mass at five lattice spacings **0.460(30)**.

$\beta = \mathbf{6}$	$am \ [\bar{t}]$	c	c'
A_1	1.190(24)[1.5]	1.000(10)	0.017(14)
A_1^*	1.804(96)[1.5]	0.990(21)	0.142(28)
A_3	1.666(81)[1.5]	1	0

$\beta = \mathbf{9}$	$am \ [\bar{t}]$	c	c'
A_1	0.7731(79)[1.5]	1.000(14)	0.028(21)
A_1^*	1.179(37) [1.5]	0.998(10)	0.063(16)
A_1^{+**}	1.433(64)[1.5]	0.973(25)	0.231(32)
A_1^{+***}	1.70(13) [1.5]	0.786(98)	0.618(12)
A_3^+	1.303(47)[1.5]	1	0

$\beta = \mathbf{12}$	$am \ [\bar{t}]$	c	c'
A_1	0.572(15) [2.5]	1.000(18)	0.000(25)
A_1^*	0.856(53) [2.5]	0.992(26)	0.124(37)
A_1^{**}	0.943(39) [2.5]	0.988(38)	0.152(53)
A_1^{***}	1.294(59) [1.5]	0.680(68)	0.734(97)
A_2	1.365(57) [1.5]	0	1
A_3	0.990(60) [2.5]	1	0
A_4	1.03(10) [2.5]	0.999(32)	0.035(21)
E^-	1.547(72) [1.5]	0	1
E^+	1.650(65) [1.5]	0	1

$\beta = \mathbf{14.5}$	$am \ [\bar{t}]$	c	c'
A_1	0.489(13) [2.5]	1.000(41)	0.016(58)
A_1^*	0.669(24) [2.5]	0.998(16)	0.0619(22)
A_1^{**}	0.816(56) [2.5]	0.985(40)	0.172(56)
A_1^{***}	1.11(12) [2.5]	0.577(48)	0.816(68)
A_2	1.04(12) [2.5]	0	1
A_3	0.776(34) [2.5]	1	0
A_4	0.71(13) [3.5]	0.995(30)	0.097(27)
E^+	1.40(38)[1.5]	0	1
E^-	1.52(53)[1.5]	0	1

Table 3: Strategy II: The local effective masses, and Fourier coefficients obtained at $\beta = 6, 9, 12$ and 14.5 . The wave function coefficients c and c' , all obtained at two lattice spacings, correspond respectively to the smallest and second-smallest spin wave function compatible with the lattice representation (e.g., $c = c_0$ and $c' = c_4$ for the A_1 representation). The number in brackets indicates at what time separation the local effective mass was evaluated.

State	$L = 16$	$L = 24$	$L = 32$
0^+	0.764(11)	0.7681(93)	0.766(27)
0^{+*}	1.065(21)	1.159(28)	1.113(48)
2^+	1.194(22)	1.287(47)	1.295(62)
4^+	1.620(37)	1.623(66)	1.57(13)

Table 4: Strategy I: volume dependence of various glueball masses in lattice units at $\beta = 9$

β	L	$a\sqrt{\sigma}$
6.0	16	0.2538(10)
9.0	24	0.1616(6)
12.0	32	0.1179(5)
14.5	40	0.09713(20)

Table 5: The string tension values obtained in [9]

State	$m/\sqrt{\sigma}$	C.L.[%]
0^+	4.76(11)	99
0^{+*}	6.88(23)	14
2^+	8.44(24)	99
2^-	8.81(34)	90
4^+	10.28(81)	94
4^-	10.70(93)	97

Table 6: Strategy I: Continuum extrapolation of the spectrum in units of the string tension obtained with strategy I.

State	$m/\sqrt{\sigma}$	C.L.[%]
0^+	4.934(98)	50
0^{+*}	7.03(26)	55
0^{+**}	7.54(70)	36
2^+	8.65(33)	38
4^+	11.6(1.3)	84

Table 7: Strategy II: we obtain here the following continuum-extrapolated glueball masses, in units of the string tension. The continuum quantum numbers have been attributed after extrapolation of the Fourier coefficients.

